U.S. DEPARTMENT OF THE INTERIOR
U.S. GEOLOGICAL SURVEY

Hydrothermal Alteration Mineralogy of SOH Drill Holes, Kilauea East Rift Zone Geothermal Area, Hawaii

By Keith E. Bargar[1], Terry E.C. Keith[2], Frank A. Trusdell[3], S. Rene Evans[4], and Martha L. Sykes[5]

Open-File Report 96-0010

[1]U.S. Geological Survey, 345 Middlefield Road, Menlo Park, CA 94025, M/S 910, U.S.A.
[2]U.S. Geological Survey, Alaska Volcano Observatory, 4200 University Drive, Anchorage, AK 99508-4667, U.S.A.
[3]U.S. Geological Survey, Hawaii Volcano Observatory, P.O. Box 51, Hawaii National Park, HI 96718, U.S.A.
[4]Los Alamos National Laboratory, EES-4 MS-D443, Los Alamos, NM 87545, U.S.A.
[5]University of Hawaii, 2525 Correa Rd., Honolulu, HI 96822, U.S.A.

CONTENTS

Abstract 5
Introduction 5
Analytical methods 7
Acknowledgments 8
Hydrothermal mineralogy of the SOH drill cores 8
SOH-1 8
SOH-2 11
SOH-4 14
Fluid-inclusion data 18
SOH-1 18
SOH-2 18
SOH-4 19
Discussion and conclusions 21
References 24

FIGURES

1. Map showing the location of three SOH geothermal drill holes and the earlier HGP-A drill hole on the East Rift Zone of Kilauea volcano, Hawaii 28
2. Cross-section showing the depth of the subaerial/submarine boundary in the three SOH drill holes 29
3. Distribution of hydrothermal alteration minerals with depth in the SOH-1 drill hole 30
4. Photomicrograph of basalt breccia fragments cemented by colorless to white anhydrite in the SOH-1 drill hole 31
5-8. Scanning electron micrographs of SOH-1 drill core specimens showing:
5. A paragenetic sequence of hydrothermal minerals coating a fracture 32
6. Subhedral analcime crystals with a light dusting of smectite filling a vesicle 33
7. Tabular truscottite, platy gyrolite, and smectite coating a fracture 34
8. Twinned phillipsite with "core-bit" termination crystals coating vesicles with earlier spherical clusters of platy smectite crystals 35
9. Distribution of hydrothermal alteration minerals with depth in the SOH-2 drill hole 36
10-18. Scanning electron micrographs of SOH-2 drill core specimens showing:
10. A vesicle filling of euhedral to subhedral, trapezohedral analcime 37
11. A fracture coating of fibrous erionite crystals deposited on a tabular anhydrite crystal 38
12. Tabular and lamellar, anhydrite crystals and later honeycomb clusters of smectite crystals deposited in spaces between anhydrite cemented breccia fragments 39
13. Euhedral to subhedral adularia crystals and later cobweb-like deposits of smectite that fill open spaces in basalt 40

14. Plagioclase crystals and a later dusting of smectite filling vesicles 41
15. Fibrous, actinolite/tremolite? crystals and later clusters or books of hexagonal, chlorite crystals deposited on a fracture surface 42
16. A. Radiating spray of euhedral, acicular, epidote crystals deposited on a fracture in vesicular basalt. B. Closer view of epidote crystals in A. that are partly coated by later chlorite 43
17. Platy biotite crystals deposited in open space between earlier quartz crystals lining a fracture in basalt 44
18. Subhedral, garnet crystals deposited on a fracture with later tiny platelets of chlorite and fibrous actinolite/tremolite. Prismatic5 epidote crystals may have formed earlier than garnet 45
19. Distribution of hydrothermal alteration minerals with depth in the SOH-4 drill hole 46
20-34. Scanning electron micrographs of SOH-4 drill core specimens showing:
20. Euhedral to subhedral, tabular, heulandite crystals partly coated by botryoidal clusters of bladed cristobalite crystals 47
21. Vesicle filling containing hemispherical and radiating clusters of prismatic phillipsite crystals 48
22. Vesicle filling of radiating, platy, smectite crystal clusters euhedral and subhedral, analcime crystals, blocky prehnite crystal clusters, and a partial, thin coating of smectite 49
23. Blocky prehnite crystal clusters that formed later than platy smectite and euhedral analcime crystals 50
24. A. Radiating and hemispherical clusters of prismatic, phillipsite crystals along with pyramidal apophyllite(?) crystal clusters. B. Apophyllite(?) crystals partly coated by a fibrous mineral 51
25. Botryoidal clusters of platy crystals of an unidentified calcium silicate mineral 52
26. Honeycomb morphology of smectite vesicle fillings 53
27. Chalcopyrite cavity filling with, fibrous actinolite/tremolite, prismatic quartz, and mixed-layer chlorite-smectite 54
28. Rhombic adularia crystals lining vesicles along with smectite 55
29. Cluster of plagioclase crystals filling a cavity 56
30. Dimpled, bacteria-like particles adhering to plagioclase crystals in Fig. 29 57
31. Cubic pyrite deposited later than euhedral quartz crystals and before platy smectite on a fracture surface 58
32. Tabular, hexagonal, pyrrhotite crystals coating a fracture with earlier smectite 59
33. Cavity filling of euhedral quartz crystals, platy mixed-layer chlorite-smectite, and fibrous actinolite/tremolite(?) 60
34. Euhedral epidote crystals, later quartz crystals, and still later chlorite-smectite filling spaces between breccia fragments 61
35. Plot of depth vs. T_h measurements for anhydrite and quartz fluid-inclusion data from two depths in the SOH-1 drill hole 62

36. Plot of depth vs. T_h measurements for hydrothermal quartz fluid-inclusion data from five depths in the SOH-2 drill hole 63
37. Photomicrographs of (A) liquid-rich, secondary(?), and (B) monophase vapor and vapor-rich fluid inclusions in SOH-2 hydrothermal quartz crystals 64
38. Plot of T_h measurements vs. salinity for fluid inclusions in hydrothermal anhydrite, calcite, and quartz crystals from the SOH drill holes 65
39. Plot of depth below mean sea level vs. salinity of fluid inclusions from the SOH drill holes 66
40. Plot of depth beneath the ground surface vs. T_h measurements of fluid inclusions in hydrothermal anhydrite, calcite, and quartz crystals fro67 ten locations in SOH-4 67
41. Photomicrographs of fluid inclusions from drill hole SOH-4 showing: A. liquid-rich, secondary fluid inclusions in calcite; B. liquid-rich, secondary fluid inclusions in anhydrite; and C. liquid-rich, secondary and vapor-rich fluid inclusions in quartz 68

TABLES

1. Electron-microprobe analyses of analcime from the SOH drill holes 70
2. Electron-microprobe analyses of feldspars from the SOH drill holes 71
3. Electron-microprobe analyses of smectite and mixed-layer chlorite-smectite from the SOH drill holes 72
4. Electron-microprobe analyses of garnet and talc from the SOH-2 drill hole 73
5. Fluid-inclusion heating and freezing data for hydrothermal minerals from the Kilauea ERZ SOH drill holes 74
6. Approximate measured temperatures (in°C) at which hydrothermal minerals occur in the Kilauea ERZ SOH drill holes compared with drill holes in Iceland and other geothermal areas 75

Hydrothermal Alteration Mineralogy of SOH drill holes, Kilauea East Rift Zone Geothermal Area, Hawaii

By Keith E. Bargar, Terry E. C. Keith, Frank A. Trusdell, S. Rene Evans, and Martha L. Sykes

ABSTRACT

Thirty-eight hydrothermal minerals were identified from 356 drill-core specimens that were obtained from three Scientific Observation Holes (SOH-1, SOH-2, and SOH-4) drilled along the lower East Rift Zone (ERZ) of Kilauea Volcano, Hawaii. The minerals formed during alteration of basaltic rocks and glass by hot, circulating, waters in aquifers consisting of variable mixtures of meteoric water and sea water. Several zeolites, hydrated calcium silicates, carbonates, clays, silicates, sulfates, sulfides, and other minerals were found filling open spaces of vesicles, fractures, and between breccia fragments of the recovered drill core; many specimens that originally consisted of glass are completely altered to some of these minerals, especially clays. Several hydrothermal minerals (erionite, mordenite, truscottite, smectite, chlorite-smectite, chalcedony, anhydrite, and hematite), occur in the SOH drill holes at higher measured temperatures than the same minerals are found in geothermal drill holes of Iceland or other geothermal areas, suggesting that temperatures within the ERZ geothermal system have increased since the minerals formed. Fluid-inclusion freezing data for quartz, anhydrite, and calcite from the three SOH holes show that composition of the inclusion fluids ranges from dilute meteoric water to highly modified sea water concentrated by boiling. Comparison of measured drill-hole temperatures with fluid-inclusion homogenization-temperature data indicates that only about 15% of the fluid inclusions could have formed under the present thermal conditions. The majority of fluid inclusions studied apparently formed during one or more temperature fluctuations associated with the emplacement of nearby dikes and their subsequent cooling.

Bacteria-like particles at 1734.6 m depth in SOH-4 could be very significant because the particles occurred at much hotter temperatures (about 265°C) than the generally accepted 110°C limit for survival of bacteria. The presence of Cl in the particles suggests that they might have lived in a saline environment and did not result from contamination by the fresh water drilling fluids. We reccomend that future drilling and subsequent handling of drill hole specimens in the ERZ and elsewhere employ controls to minimize and(or) recognize bacterial contamination.

INTRODUCTION

Kilauea Volcano is one of the most active volcanoes on earth; about 90% of the surface of this young, shield volcano is less than 1.1 ka (Holcomb, 1987). During much of Kilauea's recorded history, volcanic activity was largely confined within the caldera (Holcomb, 1987); however, since 1955, numerous eruptions have occurred along Kilauea's rift zone, especially on the East Rift Zone (ERZ) (Fig. 1) (Holcomb, 1987;

Figure 1 near here

Moore and Trusdell, 1991; Moore and Kauahikaua, 1993). Frequent volcanism in the ERZ sparked an interest in geothermal exploration more than thirty years ago (Macdonald, 1973). The potential for a significant geothermal resource, estimated to be in the 500 to 700 MWe range (Olson and others 1990), resulted in the completion of about a dozen geothermal exploration drill holes in this region since 1962 (Thomas, 1987). However, drill core, which provides much valuable information about the ERZ geothermal system, previously was obtained only from portions of the HGP-A drill hole (Thomas, 1987) (Fig. 1). Limited drill core also was recovered from a deep research drill hole at the southern edge of the summit caldera of Kilauea Volcano (Fig. 1) (Zablocki and others, 1974; Keller and others, 1979; Tilling and Jones, in press).

To better understand the geochemistry, temperature and structural conditions of the ERZ geothermal resource and to monitor changes in the hydrothermal system, the Hawaii Natural Energy Institute of the University of Hawaii at Manoa drilled 3 additional Scientific Observation Holes—SOH-1, SOH-2, and SOH-4—between 1989 and 1991 at respective surface elevations of 189, 86, and 364 m above mean sea level along the ERZ (Fig. 1) (Olson and Deymonaz, 1991; Novak and Evans, 1991; Thomas, and others, 1991; Evans and others, 1994). These coreholes succeeded in demonstrating that high temperatures (206.1°, 350.5°, and 306.1°C, respectively) are present at depths of 1,684, 2,073, and 2,000 m along a substantial portion of the ERZ. In addition, the SOH-1 hole defined the northern boundary of the geothermal reservoir within which the HGP-A hole was drilled, and the SOH-4 drill hole suggests that a potential geothermal resource exists in an area previously not drilled (Olson and Deymonaz, 1992).

About 4,559 m of drill core were recovered from the 5,758 m penetrated by the 3 SOH drill holes—an average recovery rate of nearly 80 percent (Evans and others, 1994). In addition, a few rock chips were obtained from intervals where core was not recovered because of drilling problems (Olson and Deymonaz, 1992), and some cuttings samples were collected from the upper part of the SOH-2 hole (Evans, 1992). Stratigraphic columns for the SOH holes show an upper subaerial section and lower submarine deposits (Fig. 2). The subaerial sections consist mostly of a'a and pahoehoe basalt flows

Figure 2 near here

with occasional basalt dike and(or) sill intrusions and a few ash beds, while the submarine sections contain pillow basalts and hyaloclastites that are intruded by mafic dikes (Evans, 1992; Novak and Evans, 1991). The break between submarine and subaerial volcanic deposits occurs abruptly in drill hole SOH-1, marked by a carbonate unit containing marine fossils at 748-m depth (Novak and Evans, 1991). In drill hole SOH-2, the submarine/subaerial interface was not recovered, but it was inferred to be within the 520- to 580-m depth interval (Evans, 1992). Between 1623- and 1768-m depth in drill hole SOH-4, a thick zone of limestone (containing marine fossils, sandy carbonate, and conglomerate with water-rounded pebbles) is interspersed with subaerial basalt flows, submarine hyaloclastites, and volcaniclastic deposits (Novak and Evans, 1991).

Recent articles provide a good review of the geology and hydrology of Kilauea Volcano and its geothermal system utilizing, in part, data from the SOH drill holes (Ingebritsen and Scholl, 1993; Kauahikaua, 1993; Moore and Kauahikaua, 1993; Moore and Trusdell, 1993). Results from the SOH drill holes also were included in a data set compiled to understand possible deleterious effects of the Hawaii Geothermal Project on the ground-water resources of the island of Hawaii (Sorey and Colvard, 1994).

Detailed stratigraphic columns have been published for drill holes SOH-2 (Evans, 1992) and SOH-4 (Trusdell and others, 1992); in addition to the lithologic descriptions of the drill core, these studies also contain temperature data and show the location of hydrothermal alteration minerals within the drill holes. The mineral identifications were based partly on 123 X-ray diffraction (XRD) analyses.

The purpose of the present study was to investigate the chemical composition, morphology, paragenesis, and formation temperatures of hydrothermal alteration minerals from the SOH holes for comparison with alteration of other drill holes in the ERZ, as well as other geothermal areas. Accordingly, we completed 285 additional XRD analyses, which resulted in identification of several hydrothermal trace minerals previously unreported and in clarification of some of the published mineral (mostly clays and zeolites) identifications. We also obtained paragenetic data from binocular and petrographic microscope and scanning electron microscope (SEM) studies; in addition, the SEM work provided information on hydrothermal crystal morphologies. The composition of several of the hydrothermal mineral phases was determined by electron microprobe. Mineral-formation temperatures for quartz, calcite, and anhydrite, and salinities of the fluids from which these minerals precipitated was determined by heating/freezing analyses of fluid inclusions. A previous publication (Bargar, Keith, and Trusdell, 1995) reported results of the fluid-inclusion studies and provided some information on the hydrothermal minerals found in the SOH core specimens.

ANALYTICAL METHODS

Relying upon the logs and photographs of core from the three drill holes, we selected for additional study 356 core specimens (54 from SOH-1, 141 from SOH-2, and 161 from SOH-4) that appear to be representative of the various types of alteration present in each of the drill holes; however, it should be noted that many of the boxes of drill core were not inspected. The sample subset from each drill hole was examined by binocular microscope and appropriate specimens were analyzed by XRD using a Norelco X-ray diffractometer (controlled by a Dapple computer-automation system) equipped with a graphite monochrometer and utilizing Ni-filtered Cu-Kα radiation. Rock and mineral specimens were prepared as air-dried slurries on glass slides for analysis between 3° and 40° 2θ; selected zeolite and clay specimens were heated in a furnace at 450° or 550°C and X-rayed a second time or were glycolated by placing the slides in an atmosphere of ethylene glycol at 60°C for 1 hour before re-X-raying.

Thirty-five hydrothermal-mineral specimens (1 from SOH-1, 12 from SOH-2, and 22 from SOH-4) were gold-palladium coated and mounted in a Cambridge Stereoscan 250 scanning electron microscope (SEM), equipped with an X-ray energy dispersive

spectrometer (EDS), to obtain detailed information on the morphology, paragenesis, and semiquantitative chemistry.

Quantitative analyses of a few selected hydrothermal minerals were obtained with an JEOL JXA-8900S/M/L electron probe microanalyzer using natural and synthetic mineral standards. Conditions employed for all carbon-coated, polished, thin-section minerals analyzed include: a sample current of 7.5 nA, a beam diameter of 20 μm, count times of 20 seconds, and an accelerating voltage of 15 kV.

Twenty-five doubly-polished thick sections (along with a few unpolished cleavage chips) of hydrothermal quartz, calcite, and anhydrite specimens were prepared from the three drill holes for determination of past subsurface temperatures and fluid salinities. Measurements of fluid-inclusion homogenization temperatures (T_h) by heating and final melting-point temperatures (T_m), determined by the freezing method (Roedder, 1962), were made using a Linkam THM 600 heating/freezing stage and TMS 90 temperature control system. Successive calibration runs, using synthetic fluid inclusions (Bodnar and Sterner, 1984) and chemical compounds with known melting points recommended in Roedder (1984), suggest that the accuracy of the homogenization temperature measurements should be within ±2.0°C and the final melting-point temperature values should be accurate to at least ±0.2°C. Salinities of the fluids trapped inside the fluid inclusions were calculated, in weight percent NaCl equivalent, by an equation given in Potter et al. (1978).

ACKNOWLEDGMENTS

We thank our USGS colleagues L. C. Calk and R. O. Oscarson for their assistance in obtaining the electron-microprobe analyses. Oscarson also helped with the scanning electron microscope studies. Comments by R. O. Fournier, G. O. Fridleifsson, J. Lowenstern, J. N. Moore, T. G. Theodore, and R. I. Tilling during various stages of manuscript preparation greatly improved the final report.

HYDROTHERMAL MINERALOGY OF THE SOH DRILL CORES

SOH-1

Only a few hydrothermal alteration minerals were identified in the lower part of the subaerial section of the SOH-1 drill core by Novak and Evans (1991), who reported abundant blue staining (amorphous silica), considerable iron-oxide staining (limonite and hematite), smectite, gypsum, calcite, and a zeolite mineral coating fractures in the subaerial lava flows. In our study, only a single sample was collected from the subaerial section of the drill core (Fig. 3). XRD analysis of a yellow-orange powdery to clayey

Figure 3 near here

fracture coating showed only tiny (~0.1 mm) pyrite crystals and white, fibrous gypsum. The gypsum formed very late and may have been produced by oxidation of the pyrite, probably following core recovery because some gypsum needles coat the outer cylindrical cored surface of the specimen.

Novak and Evans (1991) found hydrothermal alteration minerals throughout the submarine part of SOH-1; fractures are coated by smectite, blue staining, pyrite, gypsum, and(or) calcite, and amygduloidal fillings of smectite, analcime, other zeolites, and opal. They also reported that the groundmass of pillow basalts and hyaloclastites is altered to smectite; breccias, consisting of pillow lava fragments, are cemented by anhydrite (Fig. 4), and quartz crystals line open spaces (fractures, vesicles, or between breccia fragments)

Figure 4 near here

of core from the lower part of the drill hole.

In this study, all of the specimens collected from the submarine part of the SOH-1 drill hole contain Fe-rich (also Mg and Ca in EDS) smectite alteration (Fig. 3). Smectite coats fractures, vesicles, and breccia fragments (Fig. 4) where the green to dark green clay mineral (some smectite deposits have a bluish to grayish, very thin smectite veneer) is usually the earliest-formed hydrothermal mineral. Dark green smectite also replaces basaltic glass, as well as phenocryst and groundmass mafic crystals of the pillow basalts. Tiny (<0.1 mm) pyrite crystals or clusters of crystals occasionally are associated with the green smectite; the smectite usually appears to form early, but, in a few cases, the pyrite may have formed earlier.

In several specimens from the lower part of the drill hole, thin, colorless or gray to white, botryoidal silica formed later than smectite. XRD analyses of these fracture and vesicle fillings usually show the presence of both cristobalite and chalcedony (a cryptocrystalline variety of quartz); however, either of these two minerals can be the sole component of some silica crusts. Occasionally, fracture and vesicle fillings also contain clusters of small, colorless or frosted, subhedral to euhedral quartz crystals that formed later than dark green smectite.

Colorless bladed crystals or occasional white nodules of anhydrite were deposited in open spaces of fractures and cavities in the lower part of the drill hole (Fig. 3). The anhydrite formed later than smectite (Fig. 4) in some deposits, but it appears to have precipitated before a second(?) smectite generation, cristobalite, and mordenite (Fig. 5).

Figure 5 near here

Fractures and cavities in several of the collected specimens contain traces of a soft, white mineral identified as calcite by XRD or by reaction with hydrochloric acid. XRD analyses show that aragonite is the predominant carbonate phase in two specimens from the upper part of the submarine section, but no aragonite was detected at depth (Fig. 3). Both carbonates are fairly late deposits; calcite appears to have formed later than analcime in one fracture filling, but it is earlier than mordenite in other deposits.

Five zeolite (hydrous aluminosilicate) minerals—analcime ($NaAlSi_2O_6 \cdot H_2O$)[1], chabazite ($CaAl_2Si_4O_{12} \cdot 6H_2O$), heulandite, [$(Na,Ca)_{2-3}Al_3(Al,Si)_2Si_{13}O_{36} \cdot 12H_2O$] mordenite[$(Ca,Na_2,K_2)Al_2Si_{10}O_{24} \cdot 7H_2O$], and phillipsite [$(K,Na,Ca)_{1-2}(Si,Al)_8O_{16} \cdot 6H_2O$]—were identified in fractures and vesicles from the lower part of the drill hole

[1]Selected mineral formulas in this text are from Fleischer and Mandarino (1991)

(Fig. 3), where these minerals typically formed later than most other associated hydrothermal minerals. These five minerals, along with several other zeolites, are reported as common constituents of altered tuffs and amygdule fillings on Oahu (Hay and Iijima, 1968; Iijima and Harada, 1969; Fujishima and Fan, 1977). These authors report a progressive change from K-rich zeolites to Ca + Na-rich zeolites to Na-rich zeolites that is attributed to compositional changes of the percolating groundwater. They also indicate that wind-blown salt increases the Na content of the groundwater and thus the abundance of Na-rich zeolites at shallow depths.

Radiating sprays of white to colorless, needle-like, Ca-rich (Na was detected in EDS analysis of some specimens) mordenite crystals (Fig. 5), or of white, cottony, clusters of fibrous mordenite crystals, become more common in the deeper drill core specimens. Spherical clusters of colorless, tabular or bladed, Ca-rich heulandite crystals were only identified in two of the collected drill core specimens. The heulandite crystals are closely associated with mordenite, calcite, and smectite in vesicle fillings, but paragenetic relationships were not apparent. On the other hand, a good paragenetic sequence of smectite—anhydrite—analcime—heulandite—gyrolite [$NaCa_{16}(Si_{23}Al)O_{60}(OH)_5 \cdot 15H_2O$] plus truscottite [$(Ca,Mn^{+2})_{14}Si_{24}O_{58} \cdot 2H_2O$] was observed for hydrothermal minerals filling open spaces in a breccia consisting of pillow fragments from 1,440-m depth. Analcime (Na>Ca>K in EDS) commonly occurs as colorless, subhedral to euhedral trapezohedral crystals (Fig. 6), but in a specimen from

Figure 6 near here

1,389-m depth, a near-vertical fracture is coated by (in order of paragenesis) green smectite; colorless, massive analcime; colorless calcite; white to colorless, bladed gyrolite and truscottite (Fig. 7); and later smectite. Smectite (±aragonite or gyrolite) also is

Figure 7 near here

associated with white to colorless, radiating clusters of twinned phillipsite (K>Na>Ca in EDS) crystals (Fig. 8) and colorless, tabular (phacolite?) chabazite (Ca-rich) in three of

Figure 8 near here

the collected specimens. The hydrated calcium silicate minerals gyrolite and truscottite are seldom reported from geothermal drill holes. Both minerals generally are associated with zeolites in basic igneous rocks (Juan and others, 1970; Merlino, 1988).

Fracture and vesicle fillings in some of the SOH-1 core specimens from the lower part of the drill hole may contain clusters of small, colorless or frosted, subhedral to euhedral, quartz crystals that formed later than dark green smectite.

Talc was identified by XRD along with truscottite, mordenite, and anhydrite in a pillow-basalt breccia specimen containing some unaltered glass from 1,583.1-m depth. In the Philippine Tongonan geothermal field, talc occurs at temperatures near 300°C (Leach and others, 1983). This occurrence of talc is the only indication found for possible past high temperatures (≥300°C) in core from the SOH-1 drill hole. Glass-

bearing fragments and other minerals identified, exclusive of talc, are consistent with the ~175°C measured temperature at this depth in the SOH-1 drill hole. Undoubtedly, the talc-bearing basalt was exposed to an earlier episode of higher-temperature hydrothermal alteration. Later, the basalt was tectonically fragmented and one of the pieces containing talc was incorporated into the SOH-1 breccia.

SOH-2

In preliminary studies of drill cuttings and core from the SOH-2 drill hole, Evans (1992) reported that the subaerial part of this hole is composed mostly of fresh basalt (consisting predominantly of olivine and plagioclase), tephra, and glass. The only hydrothermal minerals Evans identified in this section of the drill hole are sparse calcite, anhydrite, and a blue veneer (smectite?) deposited on glass cuttings fragments. Below ~520- to 580-m depth, the recovered core specimens from the submarine section become increasingly more altered and open spaces of vugs and fractures contain "gypsum, anhydrite, calcite, zeolites, pyrite, chalcopyrite, sphalerite, pyrrhotite, analcime, adularia, albite, sanidine, epidote, amorphous silica, and crystalline quartz" (Evans, 1992, p. 158).

For the present study, no specimens were collected from the subaerial section of the SOH-2 drill hole where measured temperatures were only about 32°C (Fig. 9).

Figure 9 near here

Nearly all of the collected specimens were from the lower half of the submarine section, where temperatures recorded during drilling ranged between about 100° and 350°C (Fig. 9). Open-space fillings of colorless or white, fibrous, mordenite crystal clusters (see Fig. 5) and subhedral to euhedral crystalline (Fig. 10) to massive analcime, along with one

Figure 10 near here

specimen of white, fibrous to cottony erionite [$(K_2,Ca,Na_2)_2Al_4Si_{14}O_{36}\cdot 15H_2O$] (Fig. 11)

Figure 11 near here

from 1,265.8-m depth, were the only zeolite minerals identified in samples collected from this drill hole. Erionite was tentatively identified in palagonite-altered tuffs on Oahu (Hay and Iijima, 1968). Electron-microprobe analyses of SOH-2 analcime (Table 1)

Table 1 near here

show that the mineral contains only trace amounts of cations other than Na; in contrast, an analcime analysis from Oahu (Iijima and Harada, 1969) is a little lower in SiO_2 and Na_2O and contains substantially more CaO. Electron-microprobe analyses of mordenite from SOH-2 contain large balance errors and are not reported here. Nonetheless, the results do show that the mordenite from this drill hole is high in silica content and contains nearly equal proportions of CaO and Na_2O along with minor K_2O, SrO, and BaO.

Vesicles at 1,265.5- and 1,363.1-m depth are filled by white, densely packed, radiating, fibrous, tobermorite crystal clusters (Fig. 9) along with later green smectite. XRD analysis also shows the presence of adularia and anhydrite, respectively in the two specimens. Tobermorite [$Ca_9Si_{12}O_{30}(OH)_6 \cdot 4H_2O$] has a major (002) XRD reflection at 11.4 to 11.5 Å (Heller and Taylor, 1956) in specimens from the SOH-2 drill core. The zeolites and tobermorite precipitated later than most other hydrothermal minerals identified in this drill core. In drill core from Surtsey Volcano, Iceland, 12.5Å and 14Å forms of the mineral were found in addition to an 11.3Å form (Jakobsson and Moore, 1986). Another hydrated calcium silicate mineral, truscottite (see Fig. 7), occurs as rosettes of white bladed crystals filling vesicles in association with earlier green smectite and colorless to white analcime at 1,596.2-m depth (Fig. 9). Both tobermorite and truscottite were reported from specimens below the water table in the drill hole spudded at the summit of Kilauea (Keller and others, 1979).

White to colorless, bladed to tabular, anhydrite crystal clusters (Fig. 12) occur

Figure 12 near here

sporadically in the collected samples (Fig. 9). These crystals formed late in open spaces of fractures and vesicles and are sometimes associated with even later zeolite minerals. Very tiny, white masses of gypsum (not shown in Fig. 9) frequently were observed in the same specimens and probably formed by hydration of anhydrite. In a few samples, small, tabular, anhydrite crystals have a colorless core, but crystal edges are altered to an opaque white mineral that reacts with dilute hydrochloric acid. Calcite was identified in XRD analyses or by reaction with the dilute acid in several scattered core samples (Fig. 9).

Tiny (as large as 0.5 mm), colorless, euhedral adularia crystals (Fig. 13) (see

Figure 13 near here

microprobe analyses in Table 2) occur as open-space deposits of a few drill core

Table 2 near here

specimens between 1,252.4- and 1,838.7-m depth (Fig. 9). The adularia formed earlier than smectite in some cavities (Fig. 13), but it is usually a later mineral, indicating that there is more than one generation of smectite. An XRD analysis of a thin, colorless to white, fracture coating, at 1,437.1-m depth, shows the presence of smectite, quartz, and albite Fig. 9). A few albite crystals also were observed deeper in SOH-2 during SEM analyses (Fig. 14).

Figure 14 near here

The most abundant hydrothermal alteration minerals in the SOH-2 drill core specimens are the clay minerals. In general, these minerals also appear to be the earliest hydrothermal minerals, but tiny (<0.1 mm), pyrite crystals may have formed earlier in some deposits. Other sulfides (chalcopyrite, galena, pyrrhotite, and sphalerite) also

appear to have formed early. Various shades of green clay coat or completely fill fractures, vesicles, and void spaces between breccia fragments; green clay minerals also replace glass, mafic phenocrysts, and groundmass minerals. Based on electron-microprobe analyses, the smectite-group mineral saponite is identified as the dominant clay mineral in core specimens from above 1,760-m depth (Table 3). The microprobe

Table 3 near here

analyses of two smectite specimens from SOH-2 show some variability in the chemistry, with Mg being the dominant cation in one sample and Fe most abundant in the second (Table 3). Most of the smectite deposits appear to consist of cobweb-like masses (Fig. 13) or platy crystals Fig. 12) having sharp (well-crystallized) ~15Å (001) XRD reflections that expand to ~17Å following glycolation, and collapse to ~10Å after overnight heating in a furnace.

A single core specimen from a depth of 1,503.9 m contains a white to pale green, waxy, fracture filling characterized by a 7.4Å major XRD reflection, suggesting that the clay is a member of the kaolinite-serpentine group. EDS analysis showed the presence of Mg, Si, and Fe along with traces of Ca and Al.

Green, euhedral, hexagonal, chlorite crystals (Mg, Fe, Al, and Si in EDS) or books of crystals (Fig. 15) occur in the lower part of the drill hole. Below 1,760-m

Figure 15 near here

depth, chlorite is the predominant clay mineral; however, saponite occurs in occasional core specimens and randomly interstratified chlorite-smectite was frequently identified from XRD analyses (Fig. 9). Mixed-layer chlorite-smectite has in the past been referred to as "swelling chlorite" because it has an (001) reflection that varies from ~14-14.5Å and expands to ~15-17Å after ethylene glycol treatment. There is also a slight expansion of the ~7Å reflection. Studies of chlorite-smectite specimens from Icelandic geothermal drill holes were subdivided into several types based on differences in XRD data (Kristmannsdóttir, 1976); such detailed analyses were not made for this study even though substantial differences in the XRD data were noted. Electron-microprobe analyses of mixed-layer chlorite-smectite from 1,782.1-m depth (Table 3) shows compositional variability that presumably results from different proportions of smectite and chlorite.

Several XRD analyses of clay minerals from near the bottom of the SOH-2 drill hole also show the presence of minor talc and occasional actinolite/tremolite (Fig. 9). The talc results from alteration of olivine and(or) pyroxene phenocrysts and groundmass crystals. Microprobe analyses of talc from 2046.5-m depth shows a very high MgO content (Table 4) that would be expected from the alteration of a Mg-rich olivine

Table 4 near here

phenocryst. Tiny (<0.1 mm long), white (colorless, very pale yellow-green, or blue-green in index of refraction oil), fibrous (see Fig. 15), actinolite/tremolite deposits on a few fractures also may have formed during alteration of pyroxene. Two specimens collected

from the lower part of the drill hole contain radiating sprays of tiny, green, epidote crystals that formed earlier than chlorite at 1,842.8-m depth (Fig. 16A, B). These three

Figure 16 near here

minerals (talc, actinolite, and epidote), along with chlorite, are commonly associated with low-grade greenschist facies metamorphism (Phillips and Griffen, 1981). The three minerals occur at temperatures extending to slightly above 300°C in the Tongonan geothermal field, Philippines (Leach *et al.*, 1983), as do the SOH-2 drill core specimens. Traces of two other high-temperature minerals, biotite (Figs. 17) and garnet (Fig. 18), also were identified from near the bottom of the SOH-2 drill hole (Fig. 9).

Figures 17 and 18 near here

White to bluish, botryoidal or massive chalcedony occurs in cavities and fractures of a few shallower core specimens collected for this study; however, tiny (usually <2 mm long), colorless, euhedral, quartz crystals are the more prevalent silica phase. The quartz generally formed later than the green clay minerals (smectite, chlorite, or chlorite-smectite) and pyrite, but traces of a later generation of green clay occasionally is perched on quartz crystals.

SOH-4

There appear to be two zeolite zones in the SOH-4 drill hole (Fig. 19). Tufts of

Figure 19 near here

white, fibrous, mordenite crystals (see Fig. 5); colorless to frosted, tabular, heulandite crystals (Fig. 20); colorless, euhedral analcime crystals; and clusters of prismatic phillipsite crystals (Fig. 21) fill open spaces between depths of about 750 and 1250 m.

Figures 20, and 21 near here

The only zeolite open-space deposits identified in deeper drill core specimens are colorless to white, intergrown, subhedral to euhedral, trapezohedral analcime crystals (Fig. 22). No wairakite is present in the XRD analyses of several specimens; however,

Figure 22 near here

electron-microprobe analyses of analcime from 1563.9-m depth shows the presence of about 1 weight percent CaO (Table 1) indicateing that it is intermediate in composition between Na-rich analcime and Ca-rich wairakite. A complete solid-solution series exists between the two minerals (Gottardi and Galli, 1985).

Four calcium-silicate minerals [prehnite—$Ca_2Al_2Si_3O_{10}(OH)_2$, tobermorite, truscottite, and xonotlite—$Ca_6Si_6O_{17}(OH)_2$] occur as open-space deposits at the same depths as the lower analcime zone (Fig. 19). Tiny, blocky, euhedral, prehnite crystal

clusters formed later than radiating sheets of smectite crystals and analcime and earlier than a thin, partial, smectite crust (Fig. 23). Colorless to frosted, radiating, needle-like,

Figure 23 near here

xonotlite crystals were observed in vesicle fillings or were identified from XRD analyses of a few specimens; an XRD analysis of vesicle fillings at 1,562.4-m depth shows the presence of tobermorite in addition to xonotlite. Five of the collected specimens contain fracture and vesicle fillings of white, bladed (sometimes radiating), hexagonal, truscottite (see Fig. 7) crystal clusters.

Possibly three additional calcium silicate minerals are closely associated with phillipsite in vugs at 744.5-m depth. Presently, none of these minerals have been identified; however, the EDS chemistry (Ca, K, Si) and crystal habit of one are suggestive of apophyllite (Fig. 24A and B). A fibrous, partial coating of the colorless, pyramidal,

Figure 24 near here

apophyllite(?) crystals in Fig. 24 consists of only Ca and Si (plus a trace of Al) in EDS. The third calcium silicate mineral (only Ca and Si in EDS) formed as botryoidal clusters of bladed crystals (Fig. 25).

Figure 25 near here

Vesicles, fractures, and open spaces between breccia fragments in the examined specimens often contain small amounts of calcite (Fig. 19). This colorless, white, or frosted mineral is usually found as blocky (up to 0.7 cm length) or bladed crystals that appear to have formed earlier than some of the zeolites, but it is later than smectite, chlorite-smectite, and quartz.

Except for the lowermost ~100 m of drill core, smectite is present as an open-space filling, replacement of mafic phenocrysts, or groundmass alteration in nearly every drill core specimen collected from SOH-4 (Fig. 19). The green smectite is well crystallized with sharp XRD reflections and commonly displays a honeycomb-like morphology (Fig. 26). Chemical analysis of smectite from 1,734.6-m depth (Table 3)

Figure 26 near here

indicates that it is a Mg- and Fe-rich saponite. XRD characteristics for this smectite-group mineral are the same as was described above for smectite from the SOH-2 drill hole. While the smectite is usually an early mineral, SEM studies show that some smectite formed later than analcime, prehnite (see Fig. 22), quartz, and pyrite, indicating that more than one generation of the clay was deposited.

Randomly interstratified chlorite-smectite was identified by XRD (as described above for the SOH-2 drill core) in a few scattered specimens from the submarine deposits and the lower part of the subaerial section of SOH-4 (Fig. 19). The green mixed-layer clay mineral occurs in similar replacement and open-space deposits as does smectite; its EDS chemistry (Fe, Ca, Mg, Al, and Si) suggests a similarity to that of chlorite-smectite

from SOH-2 (Table 3). In SEM studies, chlorite-smectite was observed to occur later than quartz and adularia, and chalcopyrite (Fig. 27), and it formed earlier than anhydrite.

Figure 27 near here

Small amounts of chlorite appear to be present in XRD analyses of both smectite and chlorite-smectite from the submarine section of SOH-4 (Fig. 19). The ~7Å (002) chlorite (plus smectite or chlorite-smectite) reflection splits into two peaks following glycolation, but the ~14Å (001) chlorite reflection is masked by reflections of other clay minerals.

Four silica minerals [opal, cristobalite (see Fig. 20), chalcedony, and quartz] were identified as open-space deposits in many of the SOH-4 drill hole specimens (Fig. 19). The first three minerals are found mostly above 1,250-m depth and are similar in appearance (white to frosted, botryoidal or horizontally deposited silica); however, they are readily distinguished by XRD. Quartz occurs primarily as tiny (<0.5 cm), colorless, euhedral or subhedral crystals that formed earlier (except in some green clay deposits) than associated hydrothermal minerals.

Colorless to white, euhedral, adularia (Fig. 28) and albite crystals (Fig. 29) were

Figures 28 and 29 near here

identified by XRD or SEM in fracture and vesicle fillings in a few specimens scattered through the lower half of the drill hole (Fig. 19). Both minerals appear to be closely associated with earlier quartz crystals and later smectite. Microprobe analyses of adularia and albite from SOH-4 samples are given in Table 2.

In Figure 29, there is a light to moderate dusting of later particles on top of the albite crystals. Most of the particles are clay or albite fragments, but some are similar in size and morphology to bacteria (Fig. 30). EDS analysis indicates that Cl is present in the

Figure 30 near here

collapsed-spherical or dish-shaped particles which suggests that the bacteria(?) lived *in situ* in the sea water pore fluids and may not be contamination. SEM and fluid inclusion studies of hydrothermal minerals in drill core from the Medicine Lake volcano geothermal area in northern California have yielded very similar bacteria-like particles (plus rod-shaped and branching, filamentous forms) trapped within (Bargar, 1992) or adhering to the crystal faces of hydrothermal minerals. Unfortunately, controls to permit recognition of bacterial contamination were not employed during drilling or subsequent handling of the drill core from either location. Even though we cannot determine if the bacteria-like particles are due to contamination or actually lived on the albite crystals, it would be highly significant if the particles from SOH-4 were not contaminants because the measured temperature at the depth (1,734.6 m) where these particles occur is about 265°C. Presently, about 110°C is the highest temperature at which bacteria are known for certain to survive (Huber *et al.*, 1989); however, some studies (Baross and Deming, 1983) have suggested that temperature limits above 250°C might be possible. The implication that thermophilic bacteria could have lived at high temperatures in the pore fluids

penetrated by the SOH-4 drill hole is mentioned here in order to alert others to the possibility of such occurrence, in the hope that strict controls to eliminate bacterial contamination might be employed in future drilling operations.

Colorless to white, blocky or tabular, anhydrite crystals were identified in several open-space fillings, mostly from the submarine section of the drill hole (Fig. 19). The anhydrite formed later than most other associated hydrothermal minerals; however, a few specimens contain still later, needle-like or fibrous, gypsum (not listed in Fig. 19) crystals which may originate owing to hydration of anhydrite.

Tiny, cubic, pyrite crystals (Fig. 31) were observed in several of the specimens

Figure 31 near here

collected from the lower part of the subaerial section of SOH-4 (Fig. 19). Most pyrite occurs as open-space fillings, but a few core samples contain disseminated pyrite crystals. One fracture surface at 1,281.5-m depth is lined by several bronze, hexagonal crystals that were identified as pyrrhotite by XRD and SEM (Fig. 32). The fracture surface also

Figure 32 near here

contains later smectite and calcite, as well as quartz and gypsum. Five open-space fillings near the bottom of the drill hole contain tiny (~0.1 to 0.2 mm), subhedral, reddish, tarnished, chalcopyrite (Cu, Fe, S in EDS) crystals. The chalcopyrite appears to be an early hydrothermal mineral; from SEM studies it apparently formed earlier than actinolite and chlorite-smectite (see Fig. 27).

Mafic minerals in several core samples from the subaerial part of the drill hole are altered to green and red clay. XRD analyses for two of these clay specimens indicate that the red alteration consists of hematite. A few mafic minerals (olivine?) and one cavity filling in the submarine section are partly altered to talc (Fig. 19).

Traces of an amphibole phase were tentatively identified as actinolite/tremolite in two core specimens from near the bottom of the drill hole (Fig. 19). One XRD analysis of smectite from 1,917.5-m depth shows reflections for an amphibole. Also, SEM studies of hydrothermal minerals from 1,935.8-m depth also show a fibrous mineral associated with earlier chalcopyrite (see Fig. 27), quartz, and chlorite-smectite (Fig. 33). EDS

Figure 33 near here

semiquantitative analysis of two different specimens from this sample depth suggest that the mineral might be tremolite; however, there appear to be variations in the chemistry of the fibrous mineral (Ca, Mg, Si for one analysis and Mg, Fe, Ca, Al, and Si for the other).

One brecciated core specimen from 1,971.3-m depth contains tiny, green, euhedral, epidote crystals along with later quartz (Fig. 34), and chlorite-smectite; adularia

Figure 34 near here

and chalcopyrite also are present in this core sample. The epidote consists primarily of Ca, Fe, Al, Si in an EDS analysis.

FLUID-INCLUSION DATA

SOH-1

Fluid inclusions were located only in one anhydrite specimen from 1,526.8-m depth. Fourteen T_h measurements for these liquid-rich, secondary fluid inclusions are between 157° and 161°C, which are only slightly higher than the present measured temperature at this depth (Fig. 35). The T_h values also are within the range reported

Figure 35 near here

below for one quartz crystal from deeper in this drill hole. A single T_m measurement obtained for anhydrite indicates a lower salinity (2.2 weight percent NaCl equivalent) than for the deeper hydrothermal quartz crystal which appears to have trapped sea water (Table 5); probably the anhydrite precipitated from a mixture of sea water and meteoric

Table 5 near here

water that percolated down through the volcano.

One quartz crystal from 1,654.9-m depth has very tiny (~5-10 μ), secondary, fluid inclusions. Homogenization temperature values for 9 of these liquid-rich fluid inclusions range between 155° and 171°C (Fig. 35 and Table 5). The fluid inclusions have a eutectic temperature (T_e) of ~-22°C indicating that the fluid is a NaCl solution (Shepherd and others, 1985); freezing studies show that the liquid trapped inside the fluid inclusions has a salinity of about 3.4 or 3.6 weight percent NaCl equivalent which is nearly the same as the salinity of sea water (Williams, 1962).

SOH-2

Fluid-inclusion heating and freezing data were obtained for quartz specimens from 5 depths in the SOH-2 drill hole (Table 5). Minimum T_h values for the upper 4 quartz specimens plot about 8° to 14°C below the measured temperatures at the sample depths, and maximum T_h measurements are nearly coincident with the measured temperatures for 3 of the 4 sample depths (Fig. 36). This data suggests that the fluids trapped within

Figure 36 near here

the fluid inclusions at these 4 sample depths very likely are representative of the present-day geothermal waters. Further, it appears that this thermal water is slightly hotter than when healing began along fractures containing the liquid-rich, secondary fluid inclusions. Salinities, calculated from T_m data for these fluid inclusions (Table 5), indicate that the water within the fluid inclusions probably consists either of sea water or sea water diluted to varying degrees by meteoric water.

Fluid-inclusion data for the deepest quartz specimen, where the measured temperature is very close to the theoretical reference boiling point curve (Fig. 36), is more

difficult to understand. The T_h values range from about 17° to 59°C cooler than the measured temperature at the sample depth. Most of the fluid inclusions are liquid-rich, secondary or pseudosecondary(?) inclusions (Fig. 37A) that are estimated to contain about 10 to 20 volume % vapor; however, rare vapor or vapor-rich fluid inclusions (Fig. 37B) were observed. The presence of vapor and vapor-rich fluid inclusions may indicate

Figure 37 near here

that boiling took place at some time during or following precipitation of the quartz crystal. Boiling could not be confirmed during heating studies because T_h measurements were only obtained for the liquid-rich fluid inclusions, and the vapor and vapor-rich inclusions observed do not appear to be coeval with the liquid-rich inclusions. However, boiling is definitely indicated by freezing studies, which showed some of the liquid-rich fluid inclusions to have salinities as high as 13.7 wt. % NaCl equivalent (Fig. 38), or

Figure 38 near here

nearly four times greater than the salinity of sea water. Such concentrated salinities could exist in these fluid inclusions only if the trapped fluid is composed of sea water (or sea water mixed with meteoric water) that has been heated to the boiling point (Shepherd and others, 1985).

A wide range of salinities for fluid inclusions in quartz crystals from near the bottom of SOH-2 (Table 5 and Fig. 39) indicates that the fluid inclusions trapped

Figure 39 near here

geothermal waters consisting of different proportions of meteoric water and sea water. Furthermore, the inclusions could not have been produced from the present geothermal waters. Instead, these fluid inclusions must have formed from water that boiled at a significantly lower temperature than the present measured temperature at some time during the past history of Kilauea volcano.

SOH-4

Fluid-inclusion heating and freezing analyses were obtained for two calcite specimens from the SOH-4 drill hole (Fig. 40). In the shallower sample, the liquid-rich,

Figure 40 near here

secondary, fluid inclusions trapped meteoric water (T_m=0). T_h values range between 9° and 22°C higher than the measured temperature (Fig. 40, Table 5), suggesting that temperatures once were higher than the present-day temperature at this depth. The lower measured temperature may be due to continued influx of cool meteoric water. Conversely, at 1,886.4-m depth, the liquid-rich, secondary, fluid inclusions in calcite (Fig. 41A) have T_h values that are 25° to 44°C lower than the measured temperature for

Figure 41 near here

this depth (Fig. 40). These T_h measurements are nearly coincident with fluid-inclusion T_h values for quartz from the same sample depth. The colorless, euhedral quartz crystals, and probably also the fluid inclusions in quartz, formed earlier than the colorless, blocky, calcite crystals. The distribution of calcite fluid inclusion T_h values suggest that the fluid inclusions could have formed either during a cooling trend, or during subsequent heating that may have led to the current temperature at this depth. The calcite fluid inclusions have T_m values (Table 5) suggesting that the fluid inclusions trapped sea water, whereas higher T_m measurements indicate that quartz fluid inclusions trapped a mixture of sea water and meteoric water. Thus, even though the quartz fluid inclusions and some of the calcite fluid inclusions have the same T_h values, fluid inclusions in these two minerals could not have formed at the same time.

The above interpretations do not consider the possible effects of stretching or leakage of the calcite fluid inclusions. Studies have shown that shape and size of fluid inclusions in soft, easily cleavable minerals, such as calcite, can be altered by increases in temperature or pressure, and T_h values of the stretched fluid inclusions would increase accordingly (Prezbindowski and Larese, 1987). For this study, no attempt was made to determine whether or not the calcite fluid inclusions had been deformed. Even if some deformation did occur owing to heating following formation of the fluid inclusions, the interpretations given above, with regard to the T_h values of the calcite fluid inclusions and past temperatures, would not be changed.

Anhydrite is another soft, cleavable mineral in which fluid inclusions (Fig. 41B) might be affected by leakage or stretching. Again, other than recognition of the potential problem, no attempt was made to determine if deformation owing to overheating of the fluid inclusions in anhydrite utilized in this study had occurred. As with the calcite fluid inclusion data, the interpretation of the anhydrite fluid inclusion data would not be substantially different even if some inaccuracies in the reported T_h values were found to occur because of leakage or stretching.

Temperature and salinity data were obtained for liquid-rich, secondary fluid inclusions in anhydrite from depths of 1,452.4 and 1,472.5 m. The anhydrite fluid-inclusion T_h measurements range from 11°C below to 64°C above the present-day temperatures (Fig. 40, Table 5). The T_h values for both sample depths suggest that past temperatures have been substantially higher than the measured temperature, and that at one time the temperature at this depth was even cooler than at present. The few T_m values obtained for these fluid inclusions indicate that the trapped liquid consists mostly of meteoric water (Table 5).

T_h values for liquid-rich, secondary fluid inclusions in anhydrite (Fig. 41B) from 1,771.7-m depth are 58° to 68°C lower than the measured temperature at this depth (Fig. 40, Table 5). This fluid inclusion data and the data for calcite fluid inclusions from 1,886.4-m depth (discussed above) both suggest that the temperature at these depths is substantially hotter than when the fluid inclusions formed. Only one T_m value was obtained for anhydrite fluid inclusions. The trapped liquid in this fluid inclusion appears to be slightly more saline than sea water, although no evidence for boiling (vapor-rich fluid inclusions) was observed.

Fluid-inclusion T_h measurements were made for hydrothermal quartz crystals from six depths in the SOH-4 drill hole (Table 5) (T_h data for depths of 1,959.7, 1,969.9, and 1,973.9 m were combined in Fig. 40). The quartz T_h values range from 7° to 51°C below the measured temperature curve (Fig. 40). The majority of these fluid inclusions are liquid-rich, and appear to be secondary or pseudosecondary; however, at 1,959.7-m depth several vapor-rich fluid inclusions occur (Fig. 41C). T_h values for these vapor-rich fluid inclusions were not obtained because the volume of the vapor very gradually increased and the exact temperature during heating at which all of the liquid disappeared could not be distinguished. Even though the liquid-rich and vapor-rich fluid inclusions were not determined to be coeval, the vapor-rich inclusions probably indicate that boiling occurred at this depth. Most of the T_m measurements for the quartz fluid inclusions from this drill hole suggest mixing of meteoric water and sea water, but the salinity of the liquid trapped within some of the fluid inclusions at 1,959.7-m depth (Table 5) is substantially greater than that of sea water; this also indicates that boiling probably occurred. If true, boiling took place sometime in the past when the fluid temperature as indicated by the T_h measurements exceeded a theoretical reference boiling point curve (dotted curve in Fig. 40) originating at an altitude as much as 1 km lower than the present ground surface.

DISCUSSION AND CONCLUSIONS

Table 6 lists the hydrothermal minerals identified in this study of core specimens

Table 6 near here

from the three Kilauea SOH drill holes. Many of these minerals previously were reported from earlier drill holes in the Kilauea ERZ (Stone and Fan, 1978; Waibel, 1983; Thomas, 1987), as well as prior reports on the SOH drill holes (Novak and Evans, 1991; Evans, 1992; Trusdell and others, 1992; Evans and others, 1994). However, several additional hydrothermal minerals were identified for the first time during this detailed investigation of selected drill core samples.

Abundant data have been compiled on hydrothermal alteration of drill hole specimens from geothermal areas of Iceland (see partial listing in Table 6). The Icelandic geothermal studies are applicable to Hawaiian geothermal systems because: (1) both areas consist of basaltic lavas with similar permeabilities, (2) both systems encountered the same degree of heating, (3) they are both intruded by seawater mixed in varying amounts with meteoric water, (4) the two systems produced similar suites of hydrothermal alteration minerals, and (5) they both have experienced prograde and retrograde metamorphism owing to periods of volcanic activity with intervening periods of cooler temperatures (Tómasson and Kristmannsdóttir, 1972).

During studies of Icelandic geothermal systems, apparent formation temperatures for many hydrothermal minerals were recorded (Table 6). With some exceptions, most of the hydrothermal minerals identified from the three SOH drill holes appear to have precipitated at temperatures near that at which these minerals were deposited in Icelandic and other geothermal areas (Table 6). Gypsum occurs in at least two of the drill holes at

depths where the rock temperatures are far hotter than the temperature range (<70 °C) at which gypsum forms (Holland and Malinin, 1979). Most likely, the gypsum precipitated during or following retrieval of the drill core at the surface due to hydration of anhydrite with which it commonly is found. Erionite, tobermorite, and truscottite occur at significantly higher temperatures than drill-hole specimens from Iceland or other areas; this discrepency may be only an apparent one because the minerals are rarely reported. However, chalcedony, smectite, and mixed-layer chlorite-smectite all occur in the SOH drill holes at temperatures as high as 350°C (Table 6). In the drill holes from Iceland and other areas, these minerals are believed to have precipitated at temperatures below 240°C. Mordenite, talc, anhydrite, and hematite also are present at somewhat higher temperatures in SOH-2 than elsewhere. Therefore, we conclude that temperatures of the rocks penetrated by the SOH drill holes have increased subsequent to the formation of several hydrothermal minerals. Previous investigations of hydrothermal alteration in the ERZ have reached similar conclusions. Waibel (1983) observed similar discrepencies between the temperatures at which a few hydrothermal minerals from the HGP-A drill hole (see location in Fig. 1) occur and the temperatures at which the same minerals formed in Icelandic and other geothermal areas. Similarly, a comparison of temperatures at which hydrothermal minerals (particularly anhydrite) were found in HGP-A and several other nearby drill holes in the ERZ suggested to Thomas (1987, p. 1517) that one possible explanation might be that "the part of the rift penetrated by these wells has undergone a complex history of heating and cooling associated with successive episodes of magmatic intrusions and subsequent cooling by hydrothermal circulation".

The fluid-inclusion studies conducted for this investigation also show that there have been past fluctuations in temperatures of fluids contained in the rocks penetrated by the SOH drill holes. Homogenization temperature measurements for quartz crystals from four depths in the SOH-2 drill hole straddle the measured temperature curve for this drill hole (Fig. 9). It seems probable that these fluid inclusions formed from the present temperature conditions within the drill hole. A few anhydrite and calcite specimens from the SOH-1 and SOH-4 drill holes have T_h values that are substantially higher than the measured temperatures. The measurements suggest that past temperatures at these depths have been a few degrees to several tens of degrees hotter and subsequently cooled to the present temperatures. Additional anhydrite and calcite samples from the SOH-4 drill hole along with the remaining quartz specimens from all three drill holes have fluid inclusion T_h measurements that plot below the present measured temperature curve indicating that past temperatures also have been cooler.

Melting-point temperature measurements show that the water trapped within the SOH fluid inclusions ranges from pure meteoric water to sea water. Sea water trapped within fluid inclusions from the bottom of SOH-2 and SOH-4 must have boiled. T_m measurements for fluid inclusions in quartz crystals from these depths (Table 5) indicate that the amount of dissolved salts within some fluid inclusions exceeds that of sea water; such high salinities undoubtedly were produced by boiling. In addition, a few of the fluid inclusions are single-phase vapor or vapor plus small amounts of liquid, which also characterizes boiling conditions. If boiling did occur at these depths, the conditions that would be used to construct a reference boiling-point with depth curve must have been very different from the present-day thermal regime. The simplest explanation would be for these fluid inclusions to have formed at an earlier time when the elevation of the

ground surface in the ERZ was on the order of one kilometer lower than its current altitude. However, Kilauea is a very dynamic volcano, and the precise explanation probably is much more complex. In addition to extensive volcanism, recent studies have shown that subsidence (Moore and Thomas, 1988; Ludwig *et al*, 1991) and giant submarine landslides (Moore et al., 1989; Moore et al., 1994a, 1994b) have substantially influenced the size and shape of the Kilauea Volcano.

REFERENCES

Aumento, Fabrizio and Liguori, P. E. (1986) Conceptual reservoir models through geoscientific investigations.*Geothermics* **15**, 799-806.

Bargar, K. E. (1992) Video-tape of bacteria-like moving particles in fluid inclusions from Medicine Lake volcano, northern California. *EOS, Trans., Amer. Geophys. Union,* **73,** no. 43, 640.

Bargar, K. E., Keith, T. E. C., and Trusdell, F. A. (1995) Fluid-inclusion evidence for past temperature fluctuations in the Kilauea East Rift Zone Geothermal Area, Hawaii. *Geothermics* **24,** no. 5/6, 639-659.

Baross, J. A. and Deming, J. W. (1983) Growth of 'black smoker' bacteria at temperatures of at least 250°C. *Nature* **303**, 423-426.

Bodnar, R.J. and Sterner, S. M. (1984) Synthetic fluid inclusions in natural quartz I. Compositional types synthesized and applications to experimental geochemistry. *Geochim. Cosmochim. Acta* **48**, 2659-2668.

Cavarretta, G., Gianelli, G. and Puxeddu, M. (1982) Formation of authigenic minerals and their use as indicators of the physicochemical parameters of the fluid in the Larderello-Travale geothermal field. *Econ. Geol.* **77**. 1071-1084.

Elder, J. (1981) *Geothermal systems.* Academic Press, London, 508 pp.

Elders, W. A., Hoagland, J. R., McDowell, S. D. and Cobo, J. M. (1979) Hydrothermal mineral zones in the geothermal reservoir of Cerro Prieto. *Geothermics* **8**, 201-209.

Evans, S.R. (1992) Summary geological report and index log of the scientific observation hole #2 on the Kilauea East Rift Zone, Hawaii. *Trans. Geother. Res. Counc.* **16**, 157-166.

Evans, S. R., Keith, T. E. C., Bargar, K. E., Trusdell, F. A., Sykes, M. L., Olson, H. J., Thomas, D. M. and Novak, E. (1994) Preliminary geologic results of three scientific observation holes (SOH), Kilauea East Rift Zone, Hawaii, USA. *Proc. VIIth Int. Symp. on the Observation of the Continental Crust Through Drilling,* April 25-30, 1994, Santa Fe, New Mexico, 138-141.

Fleischer, M. and Mandarino, J. A. (1991) *Glossary of Mineral Species*, 256 pp. The Mineralogical Record, Inc., Tucson, AZ.

Fridleifsson, G. O. (1991) Hydrothermal systems and associated alteration in Iceland. *Geol. Surv. Japan* **277**, 83-90.

Fujishima, K. Y. and Fan, P-F. (1977) Hydrothermal mineralogy of Keolu Hills, Oahu, Hawaii. *Amer. Mineral.* **62**, 574-582.

Gottardi, G. and Galli, E. (1985) *Natural zeolites*. Springer-Verlag, Berlin, 409 pp.

Hay, R. L. and Iijima, A. (1968) Nature and origin of palagonite tuffs of the Honolulu Series on Oahu, Hawaii. *Geol. Soc. Amer. Mem.*, **116**, 331-376.

Heller, L. and Taylor, H. F. W. (1956) *Crystallographic data for the calcium silicates*. Her Majesty's Stationery Office, London, 79 pp.

Holcomb, R. T. (1987) Eruptive history and long-term behavior of Kilauea volcano. In *Volcanism in Hawaii* (Edited by Decker, R. W., Wright, T. L. and Staufer, P. H.), *U.S. Geol. Surv. Prof. Pap.* **1350**, 261-350.

Holland, H. D. and Malinin, S. D. (1979) The solubility and occurrence of non-ore minerals. In *Geochemistry of hydrothermal ore deposits* (Edited by Barnes, H. L.), pp. 461-508. John Wiley & Sons, New York.

Honda, S. and Muffler, L. J. P. (1970) Hydrothermal alteration in core from research drill hole Y-1, Upper Geyser Basin, Yellowstone National Park, Wyoming. *Amer. Mineral.* **55**, 1714-1737.

Huber, R., Kurr, M. Jannasch, H. W. and Stetter, K. O. (1989) A novel group of abyssal methanogenic archaebacteria (Methanopyrus) growing at 110°C. *Nature* **342**, 833-834.

Hulen, J.B. and Nielson, D. L. (1986) Hydrothermal alteration in the Baca geothermal system, Redondo Dome, Valles Caldera, New Mexico. *J. Geophys. Res.* **91**, B2, 1867-1886.

Iijima, A. and Harada, K. (1969) Authigenic zeolites in zeolitic palagonite tuffs on Oahu, Hawaii *Amer. Mineral.* **54**, 182-197.

Ingebritsen, S. E. and Scholl, M. A. (1993) The hydrogeology of Kilauea volcano *Geothermics* **22**, 255-270.

Jakobsson, S. P. and Moore, J. G. (1986) Hydrothermal minerals and alteration rates at Surtsey Volcano, Iceland. *Geol. Soc. Amer. Bull.* **97**, 648-659.

Juan, V. C., Youh, C.-C. and Lo, H.-J. (1970) The dehydration reaction of natural truscottite. *Proc. Geol. Soc. China,***13**, 34-40.

Kauahikaua, J. (1993) Geophysical characteristics of the hydrothermal systems of Kilauea volcano, Hawai'i *Geothermics* **22**, 271-299.

Keith, T. E. C., White, D. E. and Beeson, M. H. (1978) Hydrothermal alteration and self-sealing in Y-7 and Y-8 drill holes in northern part of Upper Geyser Basin, Yellowstone National Park, Wyoming. *U.S. Geol. Surv. Prof. Pap.* **1054-A**, 26 pp.

Keller, G. V., Grose, L. T., Murray, J. C., and Skokan, C. K. (1979) Results of an experimental drill hole at the summit of Kilauea volcano, Hawaii J. *Volcanol. Geotherm. Res.* **5**, 345-385

Kristmannsdóttir, H. (1975) Clay minerals formed by hydrothermal alteration of basaltic rocks in Icelandic geothermal fields. *Geologiska Föreningens i Stockholm Forhandlingar* **97**, 289-292.

Kristmannsdóttir, H. (1976) Types of clay minerals in hydrothermally altered basaltic rocks, Reykjanes, Iceland. *Jökull* **26**, 30-39.

Kristmannsdóttir, H. (1979) Alteration of basaltic rocks by hydrothermal activity at 100-300°C. *In International Clay Conference 1978* (Edited by Mortland, M. M. and Farmer, V. C.) pp 359-367. Elsevier Sci. Pub. Co., Amsterdam.

Kristmannsdóttir, H. and Tómasson, J. (1978) Zeolite zones in geothermal areas of Iceland. *In Natural Zeolites: Occurrence, Properties, Use* (Edited by Sand, L. B. and Mumpton, F. A.), pp. 277-284. Pergamon Press, New York.

Leach, T. M., Wood, C. P. and Reyes, A. G. (1983) Geology and hydrothermal alteration of the Tongonan geothermal field, Leyte, Republic of the Philippines. *Fourth International Symposium on Water-Rock Interaction*, Aug. 29 to Sept. 3, 1983, Misasa, Japan, Abs. Vol. 275-278.

Ludwig, K. R., Szabo, B. J., Moore, J. G. and Simmons, K. R. (1991) Crustal subsidence rate off Hawaii determined from $^{234}U/^{238}U$ ages of drowned coral reefs. *Geology* **19**, 171-174.

Macdonald, G. A. (1973) Geological prospects for development of geothermal energy in Hawaii. *Pac. Sci.* **27**, 209-219.

Merlino, S (1988) Gyrolite: its crystal structure and crystal chemistry. *Mineral. Mag.* **52**, 377-387.

Moore, J. G., Clague, D. A., Holcomb, R. T., Lipman, P. W., Normark, W. R. and Torresan, M. E. (1989) Prodigious submarine landslides on the Hawaiian Ridge. *J. Geophys. Res.* **94**, B12, 17,465-17,484.

Moore, J. G., Normark, W. R. and Holcomb, R. T. (1994a) Giant Hawaiian underwater landslides. *Science*. 264, 46-47.

Moore, J. G., Normark, W. R. and Holcomb, R. T. (1994b) Giant Hawaiian landslides. *Annu. Rev. Earth Planet. Sci.* **22**, 119-144.

Moore, J. G. and Thomas, D. M. (1988) Subsidence of Puna, Hawaii inferred from sulfur content of drilled lava flows. *J. Volcanol. Geotherm. Res.* **35**, 165-171.

Moore, R. B. and Kauahikaua, J. P. (1993) The hydrothermal-convection systems of Kilauea: an historical perspective. *Geothermics* **22**, 233-241.

Moore, R. B. and Trusdell, F. A. (1991) Geologic map of the lower East Rift Zone of Kilauea volcano, Hawaii. *U.S. Geol. Survey Misc. Inv. Series Map I-2225,* scale 1:24,000.

Moore, R. B. and Trusdell, F. A. (1993) Geology of Kilauea volcano. *Geothermics* **22**, 243-254.

Novak, E. A. and Evans, S. R. (1991) Preliminary results from two scientific observation holes on the Kilauea East Rift Zone. *Trans. Geotherm.Res. Counc.* **15**, 187-192.

Olson, H. J. and Deymonaz, J. E. (1991) The Hawaiian scientific observation hole program—preliminary results and status report. *Proc. 13th New Zealand Geothermal Workshop 1991*, 115-120.

Olson, H. J. and Deymonaz, J. E. (1992) The Hawaii scientific observation hole (SOH) program summary of activities. *Trans. Geotherm. Res. Counc.* **16**, 47-53.

Olson, H. J., Seki, A., Deymonaz, J. E. and Thomas, D. M. (1990) The Hawaii scientific observation hole (SOH) program. *Trans. Geotherm. Res. Conc.* **14**, pt. 1, 791-798.

Passaglia, E. (1970) The crystal chemistry of chabazites. *Amer. Mineral.* **55**, 1278-1301.

Phillips, W. R. and Griffen, D. T. (1981) *Optical mineralogy: the nonopaque minerals.* W. H. Freeman and Company, San Francisco, 677 pp.

Potter, R. W. II, Clynne, M. A. and Brown, D. L. (1978) Freezing point depression of aqueous sodium chloride solutions. *Econ. Geol.* **73**, 284-285.

Prezbindowski, D. R. and Larese, R. E. (1987) Experimental stretching of fluid inclusions in calcite—implications for diagenetic studies. *Geology*, **15**, 333-336.

Roedder, E. (1962) Studies of fluid inclusions I: Low temperature applications of a dual-purpose freezing and heating stage. *Econ. Geol.* **57**, 1045-1061.

Roedder, E. (1984) Fluid inclusions. In *Reviews in Mineralogy* (Edited by Ribbe, P. H.), vol. 12, Mineralogical Society of America, Washington, D.C., 644 pp.

Shepherd, T. J., Rankin, A. H. and Alderton, D. H. M. (1985) *A practical guide to fluid inclusion studies.* Blackie & Son, Limited, London, 239 pp.

Sorey, M. L. and Colvard, E. M. (1994) Potential effects of the Hawaii geothermal project on ground-water resources on the island of Hawaii. *U.S. Geol. Surv. Water Res. Inv. Rept.* **94-4028**, 35.

Stone, C. and Fan, P. F. (1978) Hydrothermal alteration of basalts from Hawaii geothermal project well-A, Kilauea, Hawaii. *Geology* **6**, 401-404.

Thomas, D. M. (1987) A geochemical model of the Kilauea East Rift Zone. In *Volcanism in Hawaii* (Edited by Decker, R. W., Wright, T. L. and Staufer, P. H.), *U.S. Geol. Survey Prof. Pap* **1350**, 1507-1525.

Thomas, D. M., Novak, E. A., Evans, S. R. and Olson, H. J. (1991) Scientific observation holes on Kilauea volcano. *EOS, Trans. Amer. Geophys. Union* **72**, 562.

Tilling, R. I., and Jones, B. F. (in press) Waters associated with an active basaltic volcano, Kilauea, Hawaii: variation in solute sources, 1973-1991. *Geol. Soc. Amer. Bull.*

Tómasson, J. and Kristmannsdóttir, H. (1972) High-temperature alteration minerals and thermal brines, Reykjanes, Iceland. *Contr. Mineral. Petrol.* **36**, 123-137.

Trusdell, F. A., Novak, E. and Evans, S. R. (1992) Core lithology state of Hawaii scientific observation hole 4 Kilauea volcano, Hawaii. *U.S. Geol. Survey Open-File Rept.* **92-0586**, 72pp.

Waibel, A. (1983) A review of the hydrothermal mineralogy of Hawaii geothermal project well-A, Kilauea, Hawaii. *Trans. Geotherm. Res. Counc.* **7**, 205-209.

White, D. E., Hutchinson, R. A. and Keith, T. E. C. (1988) The geology and remarkable thermal activity of Norris Geyser Basin, Yellowstone National Park, Wyoming. *U.S. Geol. Survey Prof. Pap.* **1456**, 84 p.

Williams, J. (1962) *Oceanography—an introduction to the marine sciences.* Little, Brown, and Company, Boston, 242 pp.

Zablocki, C. J., Tilling, R. I., Peterson, D. W., Christiansen, R. L., Keller, G. V., and Murray, J. C. (1974) A deep research drill hole at the summit of an active volcano, Kilauea, Hawaii. *Geophys. Res. Letters* **1**, 323-326.

1. Map showing the location of three SOH geothermal drill holes and the earlier HGP-A drill hole on the East Rift Zone of Kilauea volcano, Hawaii.

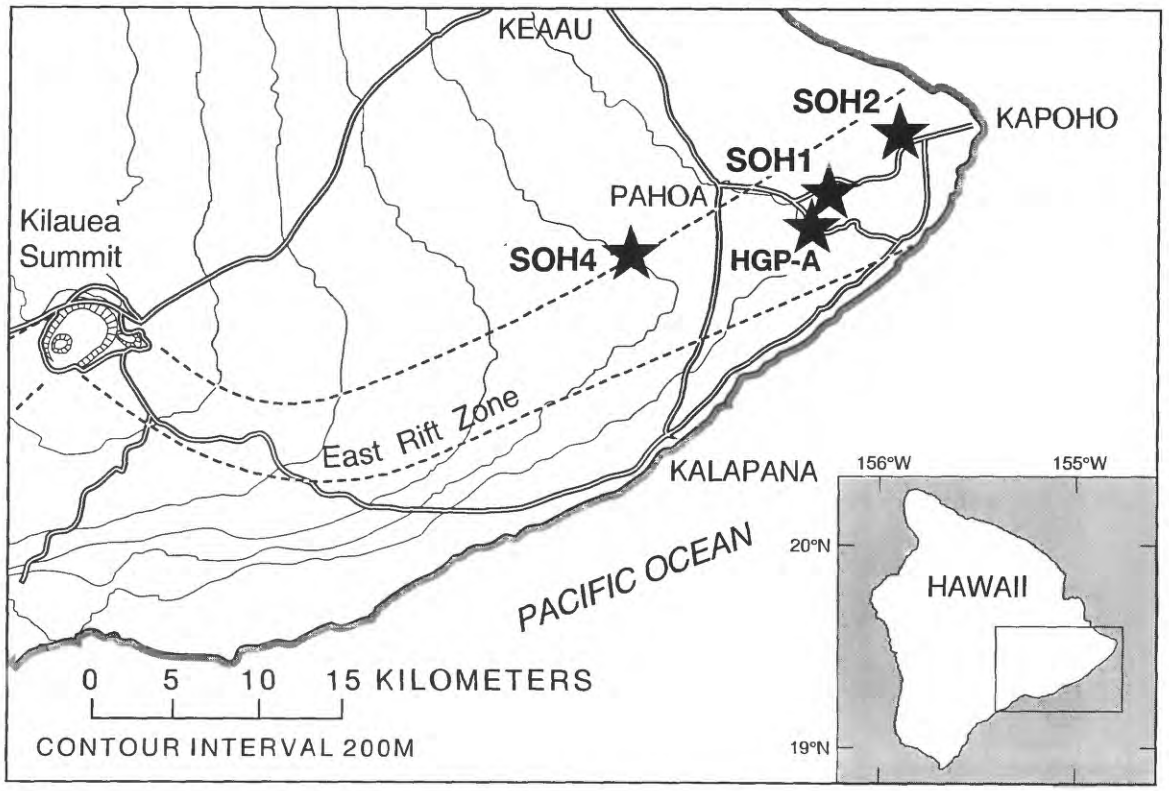

2. Cross-section showing the depth (in feet) of the subaerial/submarine boundary in the three SOH drill holes (from Evans and others, 1994).

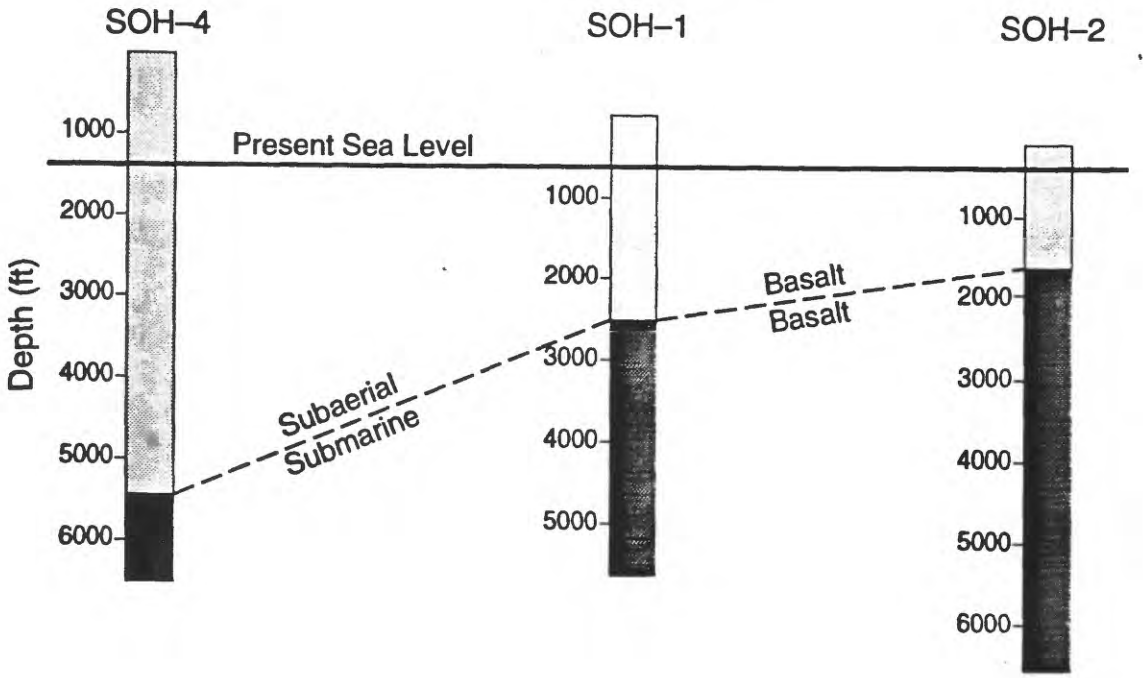

3. Distribution of hydrothermal alteration minerals with depth in the SOH-1 drill hole based on the studies of 54 collected core specimens. Temperature measurements with depth curve is shown by + symbols (Olson and Deymonaz, 1992; Novak and Evans, 1991).

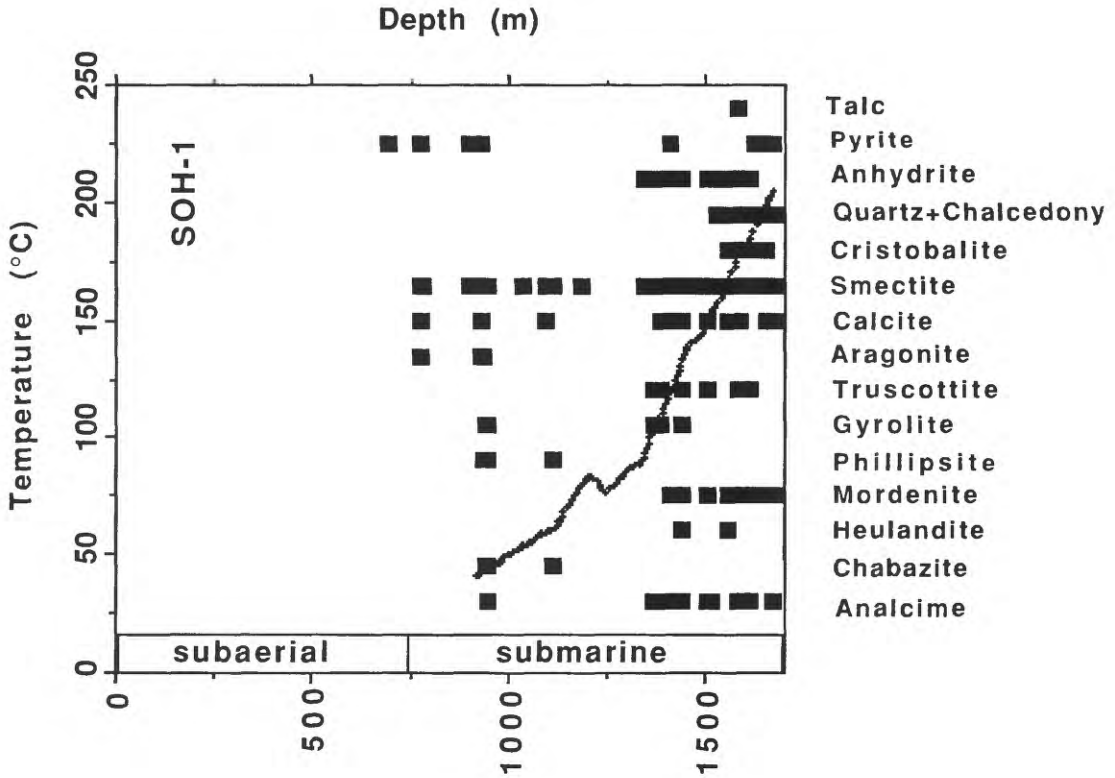

4. Photomicrograph of basalt breccia fragments cemented by colorless to white anhydrite (An) at 1,409.2-m depth in the SOH-1 drill hole. A thin rim of dark green smectite (Sm) borders each fragment.

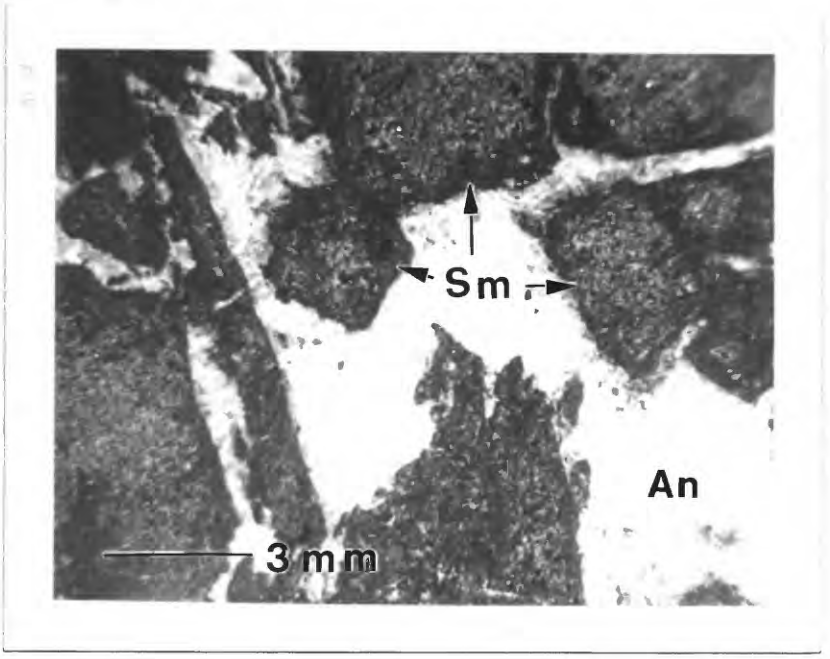

5. Scanning electron micrograph (scale on all SEM's is given in the lower left corner) showing a paragenetic sequence of hydrothermal minerals coating a fracture at 1,612.2-m depth in SOH-1. A colorless, tabular anhydrite (An) crystal contains successively later hydrothermal deposits of: white to frosted, spherical clusters of bladed cristobalite (Cr) crystals (XRD also shows the presence of chalcedony); dark green, honeycomb-appearing deposits of smectite (Sm), and white, fibrous mordenite (M).

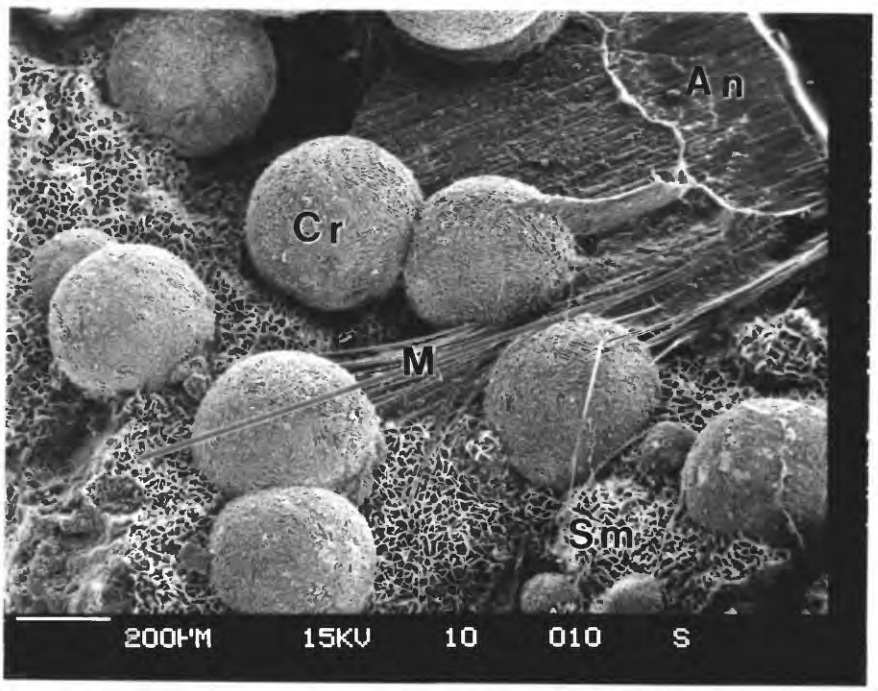

6. Scanning electron micrograph showing subhedral analcime crystals with a light dusting of smectite filling a vesicle at 948.9-m depth in SOH-1.

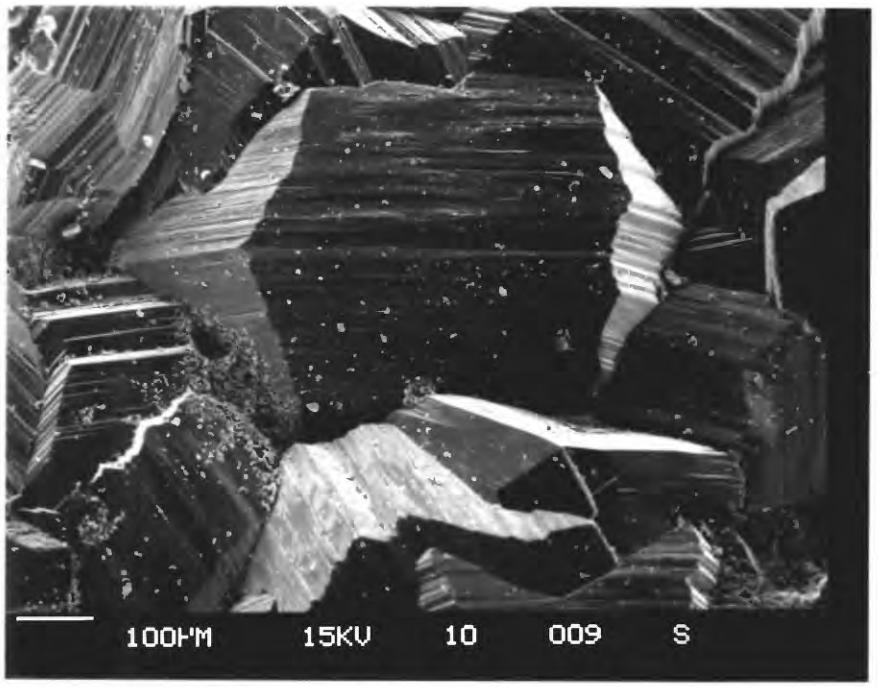

7. Scanning electron micrograph showing suhedral, tabular truscottite (Tr) along with later(?) platy gyrolite (Gy), and still later smectite (Sm) coating a fracture at 1,388.6-m depth in SOH-1.

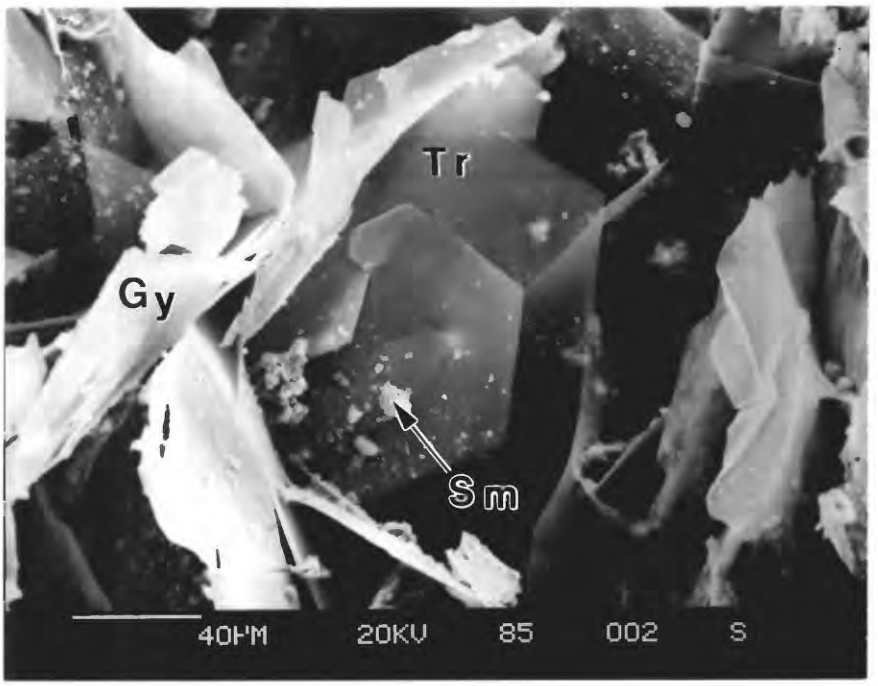

8. Scanning electron micrograph showing white to colorless, twinned phillipsite with "core-bit" termination crystals coating vesicles at 934.5-m depth in SOH-1 along with earlier spherical clusters of platy, green smectite crystals.

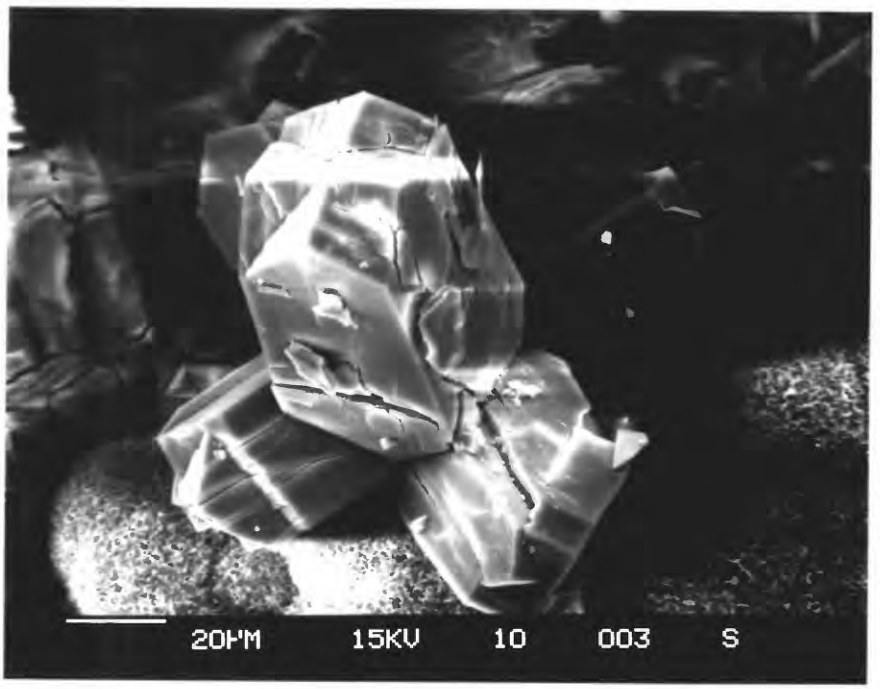

9. Distribution of hydrothermal alteration minerals with depth in the SOH-2 drill hole based on investigations of 141 collected core specimens. Temperature measurements with depth curve is shown by + symbols (Evans, 1992). Evans (1992) also presented a lithologic log and showed the distribution of hydrothermal alteration minerals identified at that time.

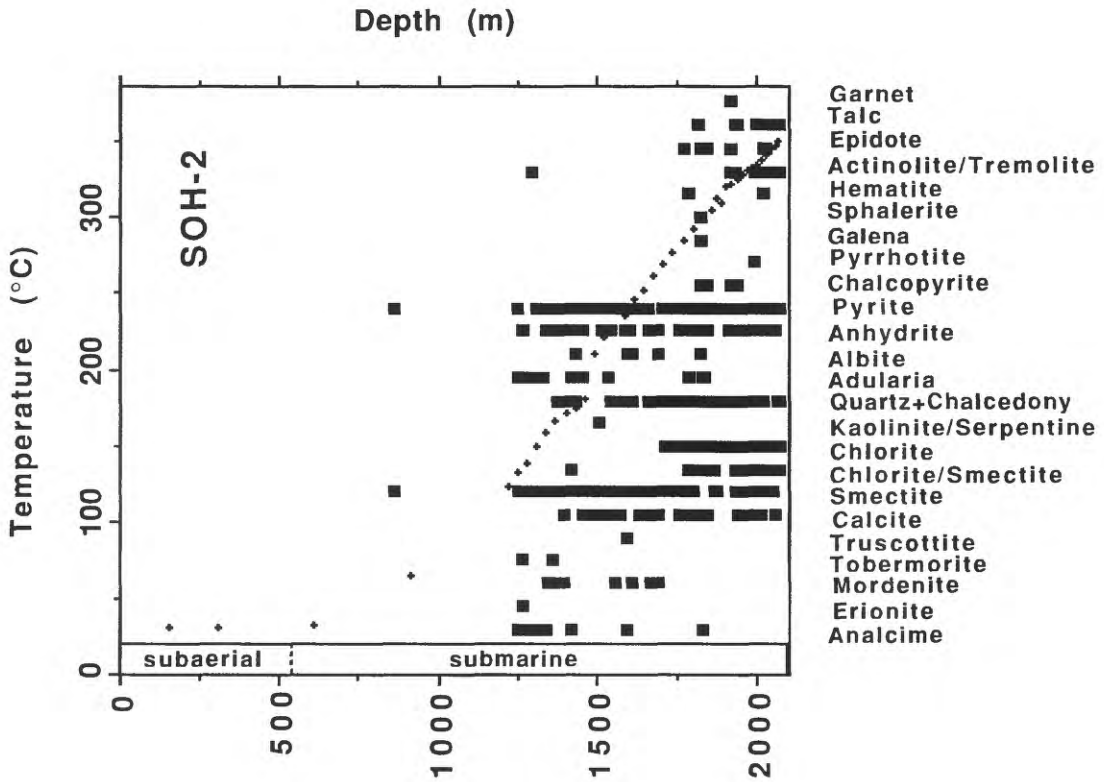

10. Scanning electron micrograph showing a vesicle filling of colorless, euhedral to subhedral, trapezohedral analcime crystals from 1,421-m depth in SOH-2. Some analcime crystals appear to have a light coating of smectite (arrow).

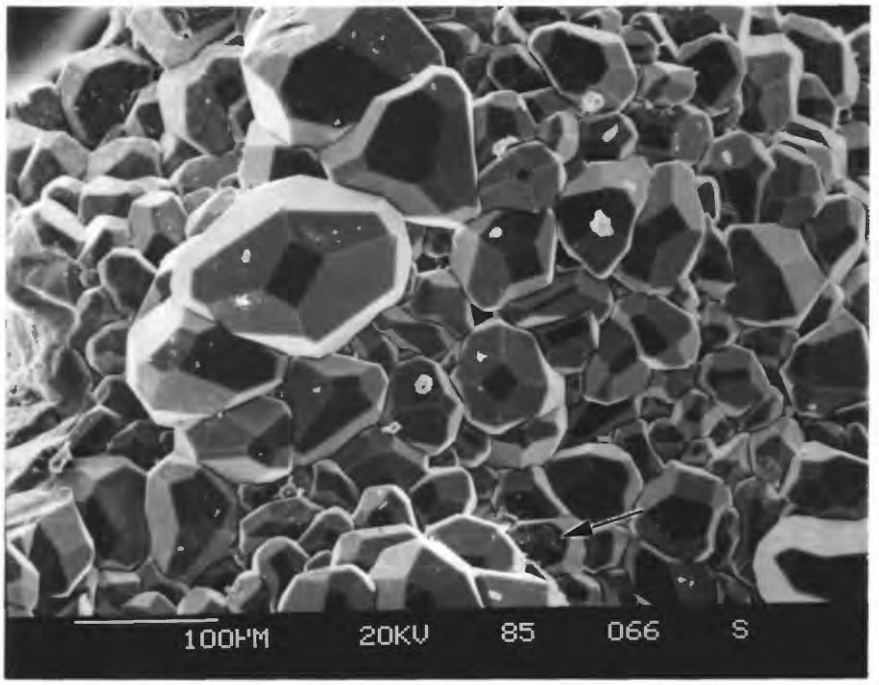

11. Scanning electron micrograph showing a fracture coating from 1,265.5-m depth in SOH-2 that consists of white, fibrous, erionite crystals deposited on a colorless, tabular, anhydrite crystal.

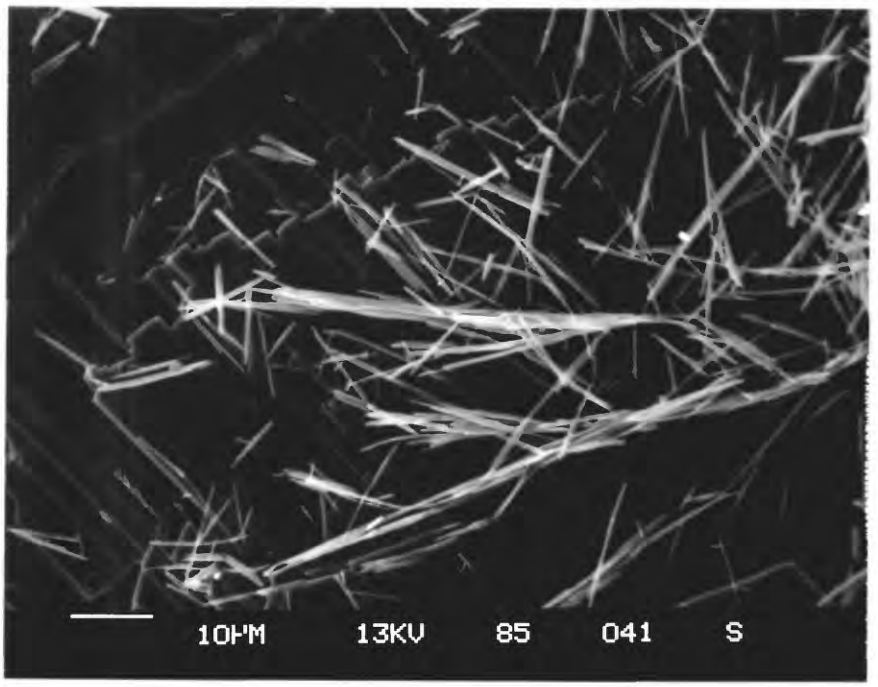

12. Scanning electron micrograph of colorless, tabular and lamellar, anhydrite crystals and later dark green, honeycomb clusters of smectite crystals deposited in spaces between anhydrite cemented breccia fragments at 1,537.8-m depth in SOH-2.

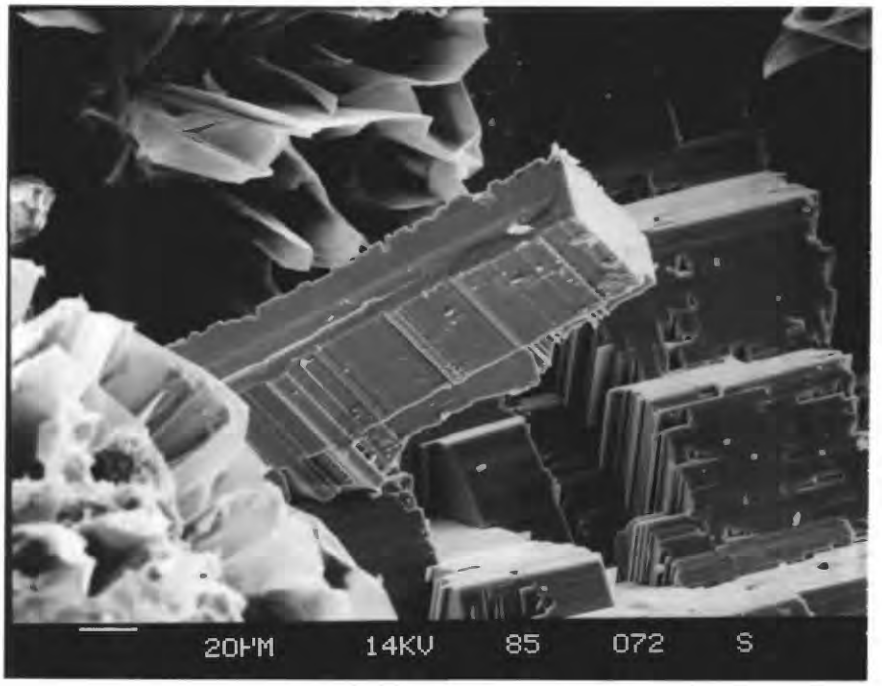

13. Scanning electron micrograph of colorless, euhedral to subhedral (some are twinned), adularia crystals and later cobweb-like deposits of green smectite that fill open spaces in basalt at 1,459.2-m depth in SOH-2.

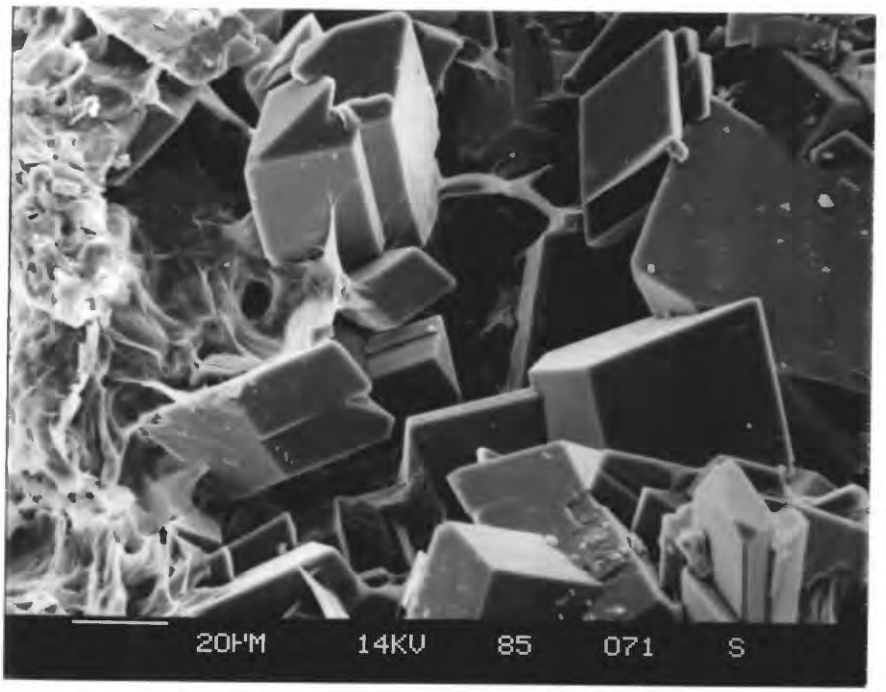

14. Scanning electron micrograph of colorless plagioclase crystals and a later dusting of smectite filling vesicles at 1,595.8-m depth in SOH-2

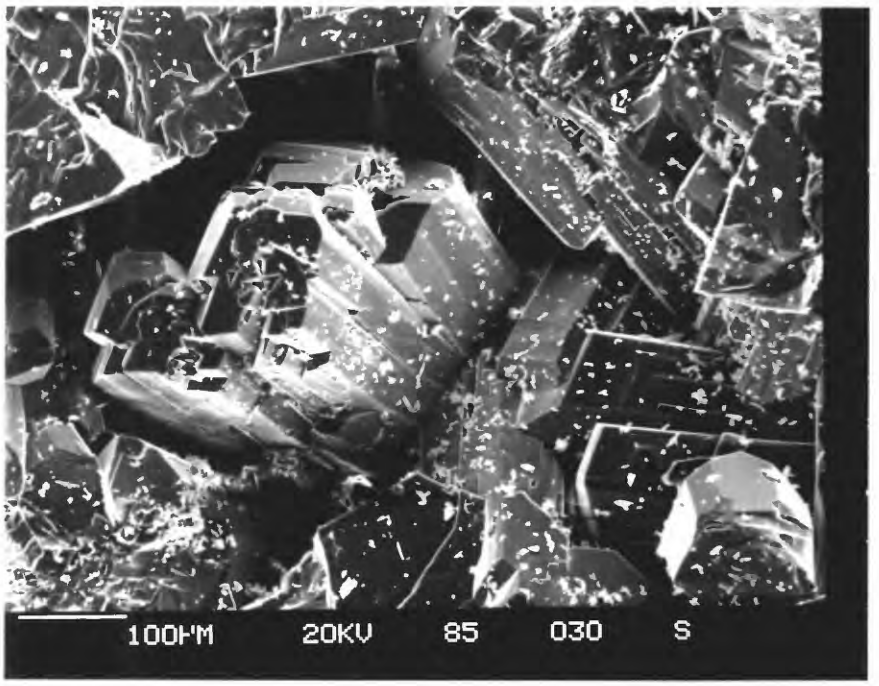

15. Scanning electron micrograph of pale green, fibrous, actinolite/tremolite(?) crystals and later clusters or books of green, hexagonal, chlorite crystals deposited on a fracture surface at 2,019.4-m depth in SOH-2.

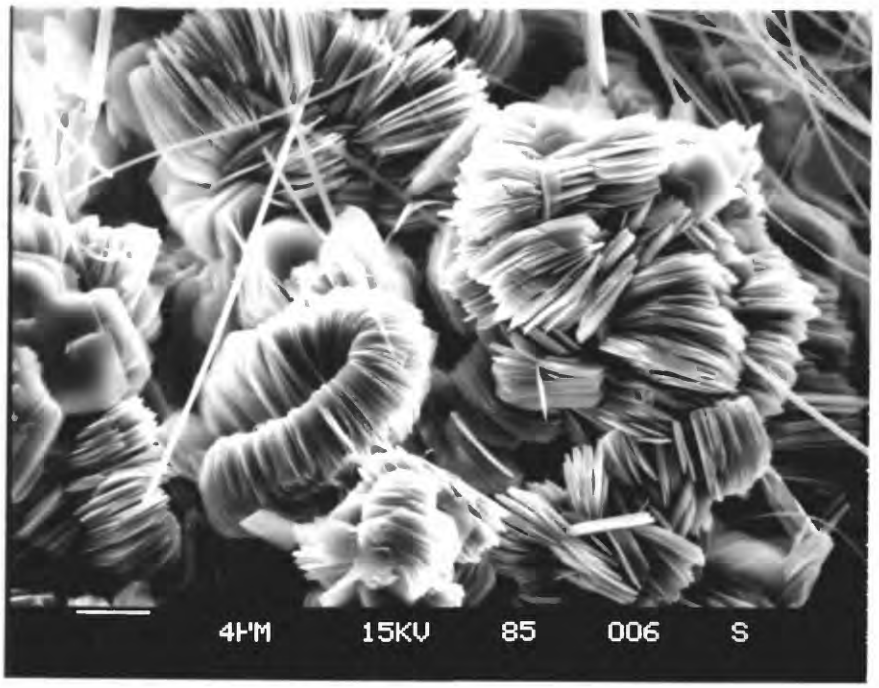

16. Scanning electron micrographs showing: A. Radiating spray of light green, euhedral, acicular, epidote crystals deposited on a fracture in vesicular basalt from 1,842.8-m depth in SOH-2. B. Closer view of epidote crystals in A. showing a partial coating of later dark green, chlorite.

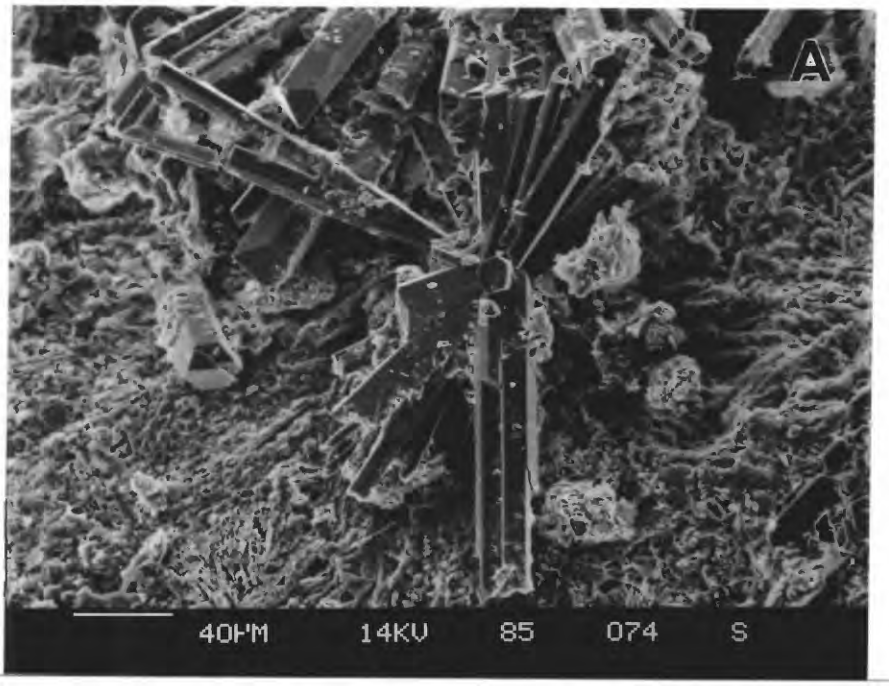

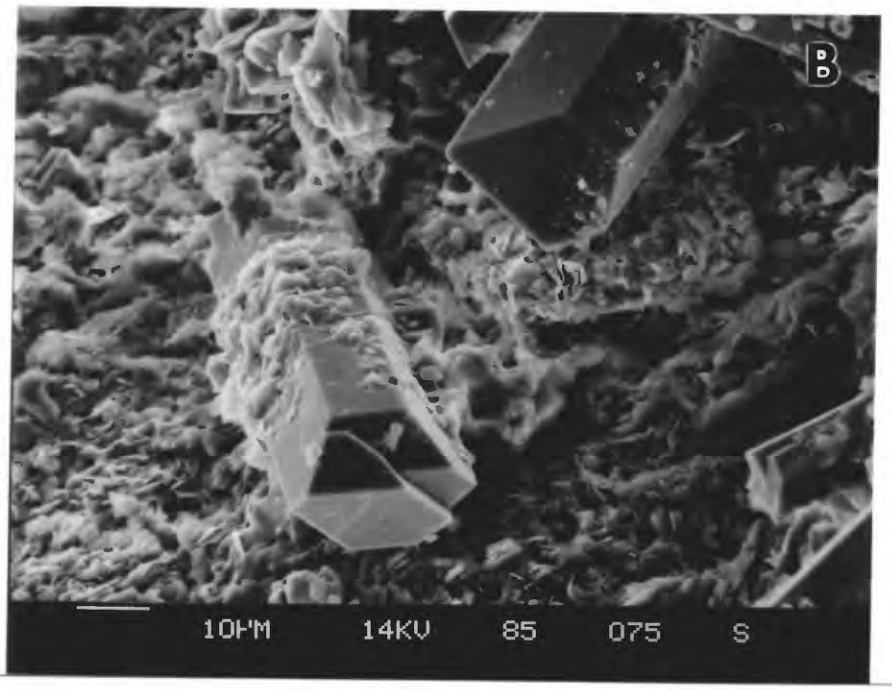

17. Scanning electron micrograph showing platy biotite crystals deposited in open space between earlier quartz crystals that line a fracture in basalt from 1,938.8-m depth in SOH-2.

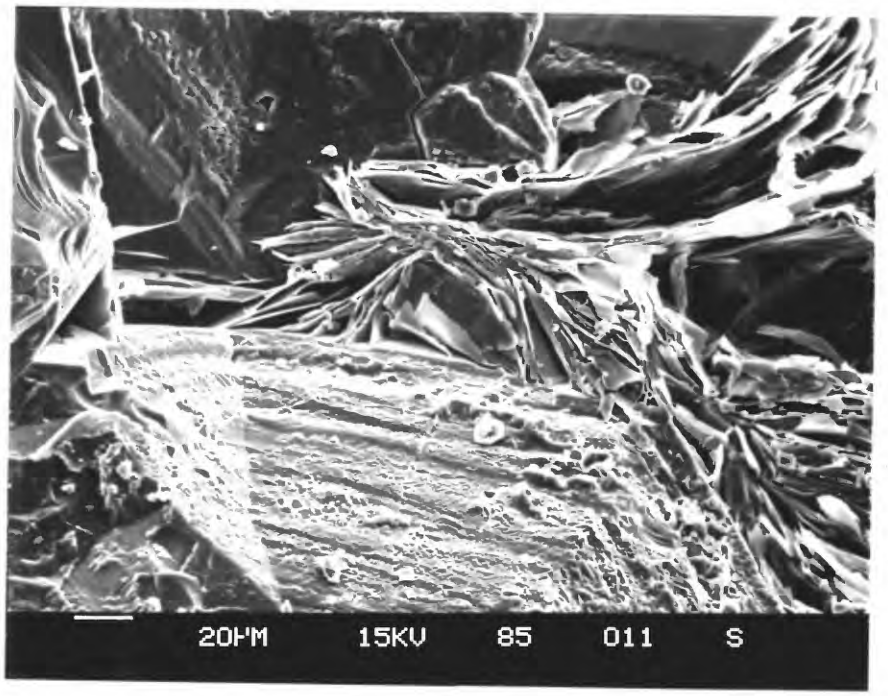

18. Scanning electron micrograph of orange, subhedral, garnet crystals deposited on a fracture at 1,918.4-m depth in SOH-2 along with later tiny platelets of green chlorite and white, fibrous actinolite/tremolite(?). Pale green, prismatic, epidote crystals (arrow) may have formed earlier than garnet.

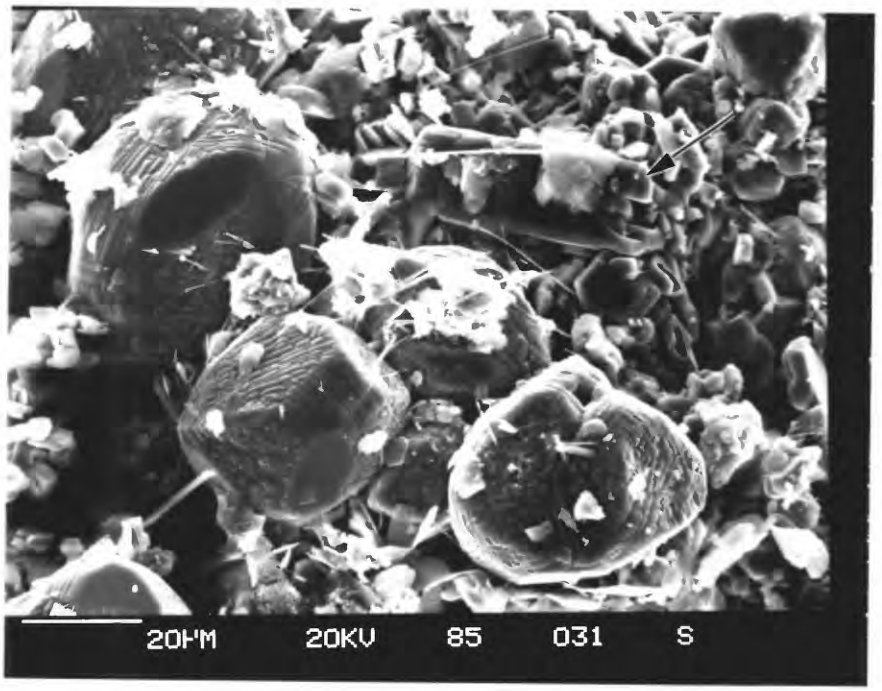

19. Distribution of hydrothermal alteration minerals with depth in the SOH-4 drill hole compiled from analyses of 161 core specimens. Trusdell and others. (1992) presented a lithologic log of core from the drill hole; they included a profile of the measured temperatures and showed the distribution of hydrothermal minerals identified at that time. The measured temperature with depth curve for this drill hole (shown by + symbols) also was given in Novak and Evans (1991) and Olson and Deymonaz (1992).

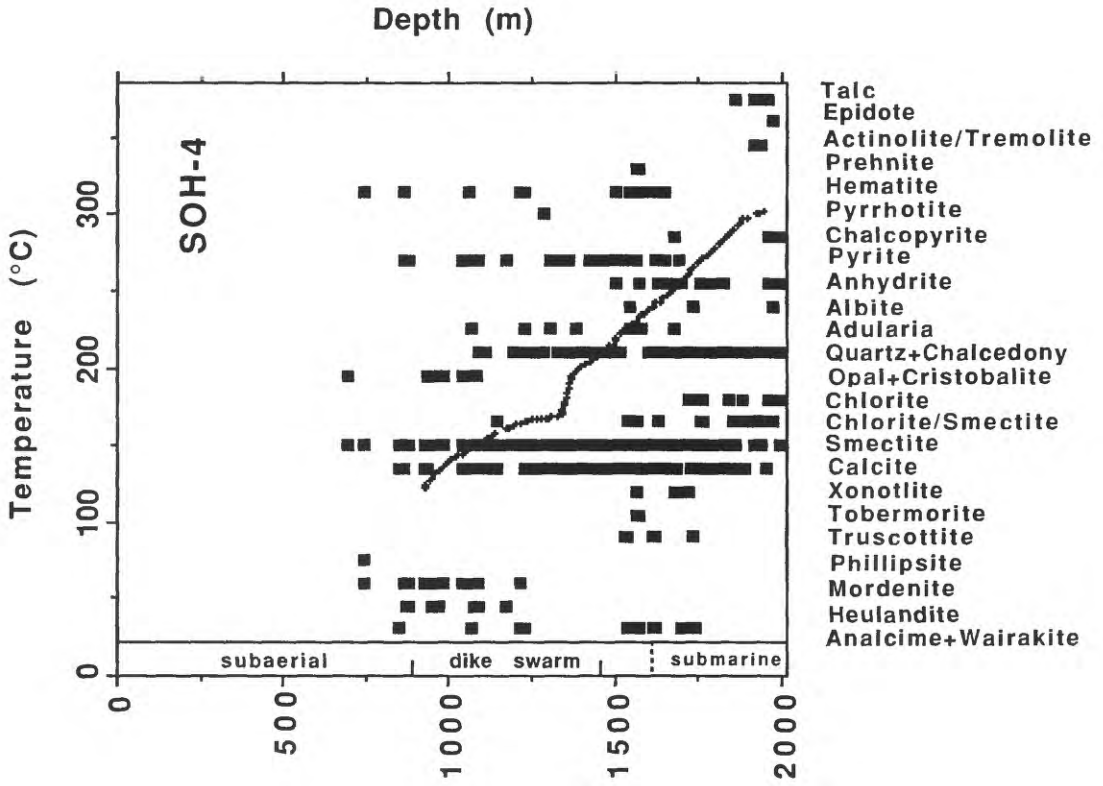

20. Scanning electron micrograph of colorless, euhedral to subhedral, tabular, heulandite crystals deposited in open spaces at 951.0-m depth in SOH-4. The heulandite crystals are partly coated by frosted, botryoidal, clusters of bladed cristobalite crystals.

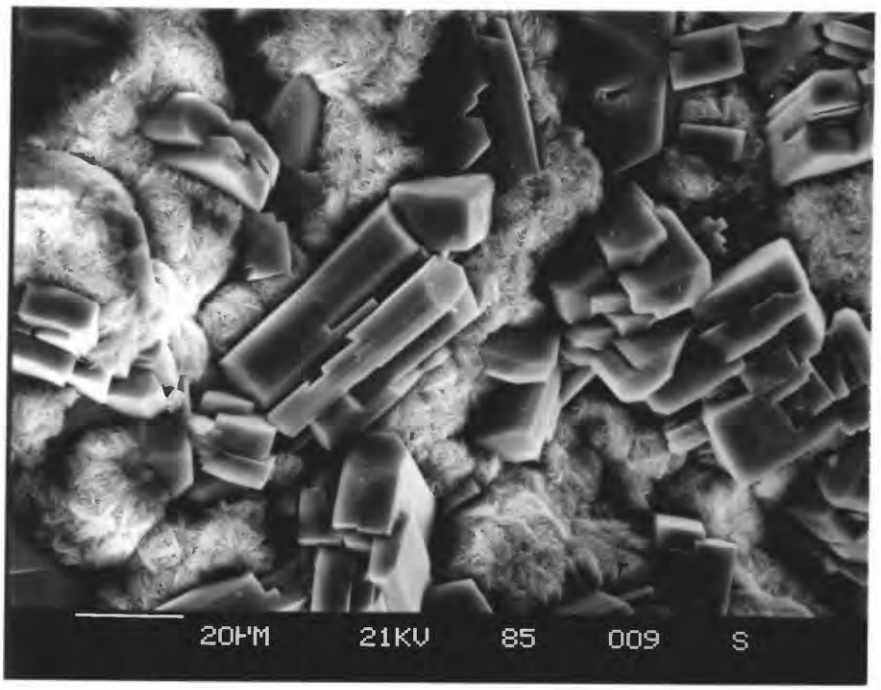

21. Scanning electron micrograph of a vesicle filling from 744.5-m depth in SOH-4 that contains hemispherical and radiating clusters of colorless, prismatic, phillipsite crystals. XRD also shows the presence of smectite.

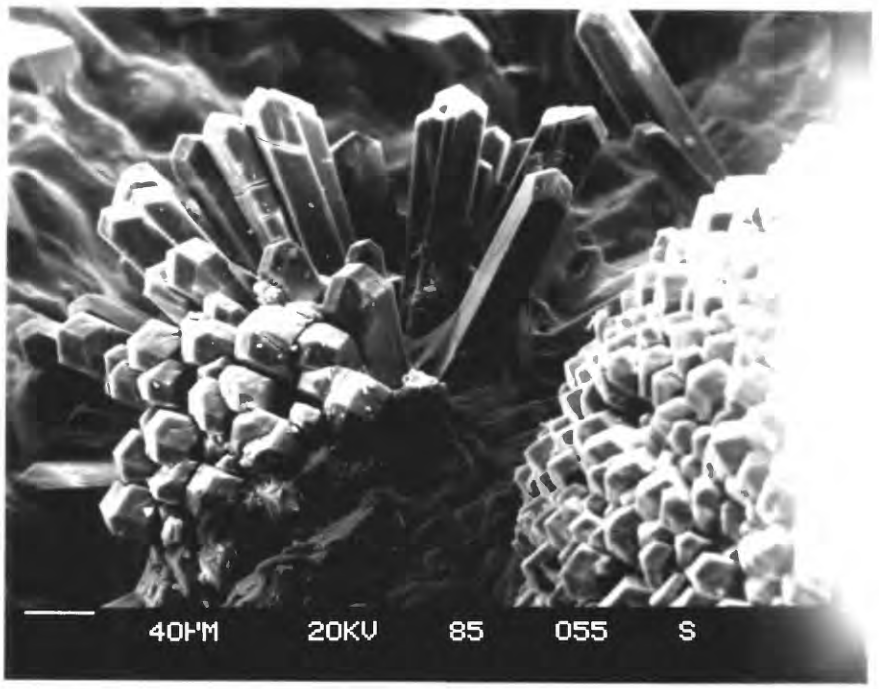

22. Scanning electron micrograph of a vesicle filling from 1,570.9-m depth in SOH-4 containing (in order of paragenesis): green, radiating, platy, smectite (Sm), crystal clusters; colorless, euhedral and subhedral, analcime (A) crystals; colorless, blocky, prehnite (Pr) crystal clusters; and a partial, thin coating of smectite (see Fig. 23).

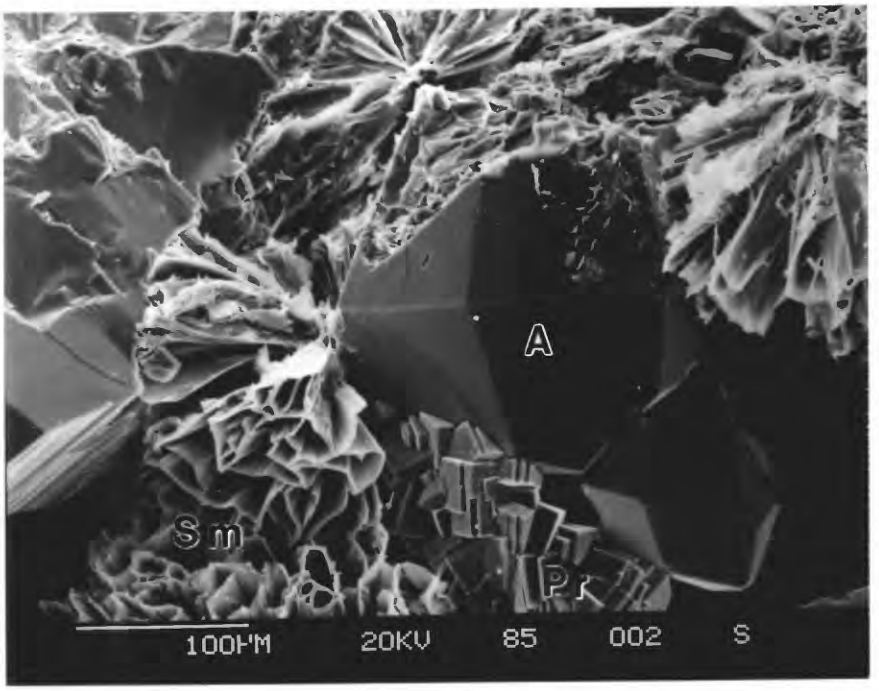

23. Scanning electron micrograph of colorless, blocky, prehnite crystal clusters that formed later than platy smectite and euhedral analcime crystals (see Fig. 22). A light dusting of smectite is the latest deposit in this vesicle filling from 1,570.9-m depth in SOH-4.

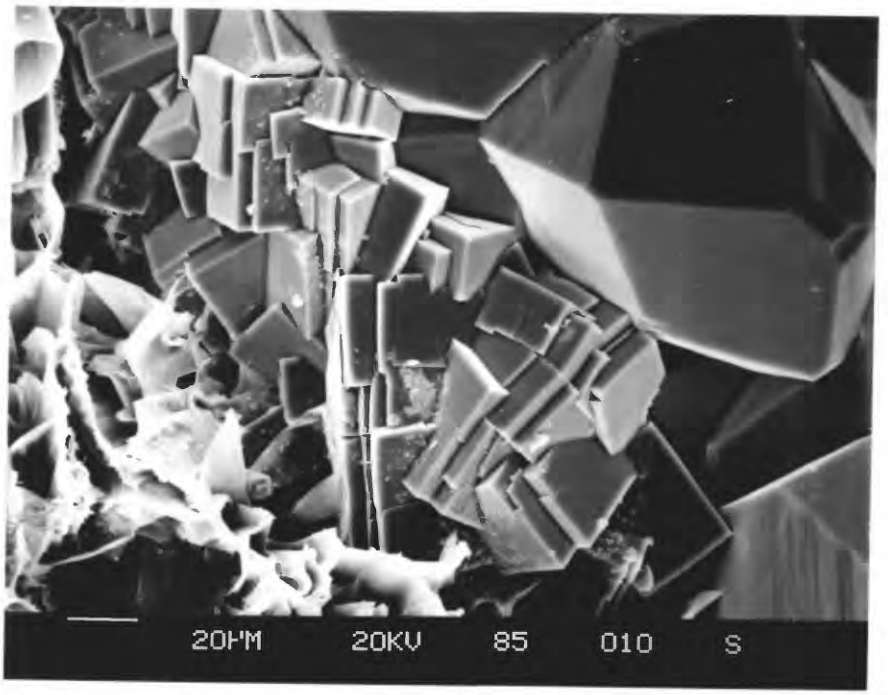

24. Scanning electron micrographs of: A. Radiating and hemispherical clusters of colorless, prismatic, phillipsite crystals (see Fig. 22) along with pyramidal apophyllite(?) crystal clusters lining vesicles in core from 744.5-m depth in SOH-4. B. The apophyllite(?) crystals are partly coated by a fibrous mineral that consists of Ca and Si (plus a trace of Al) in EDS.

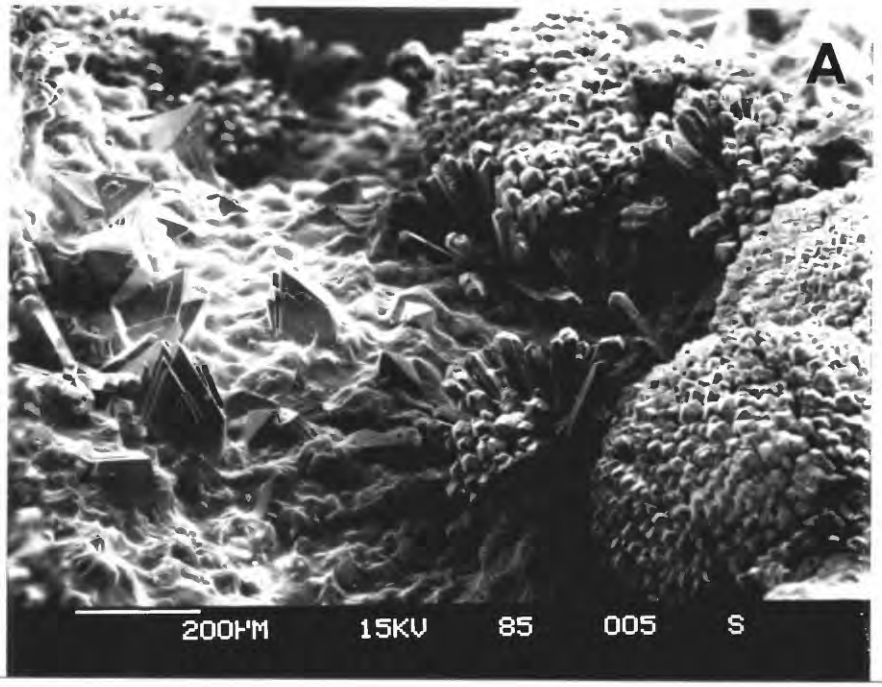

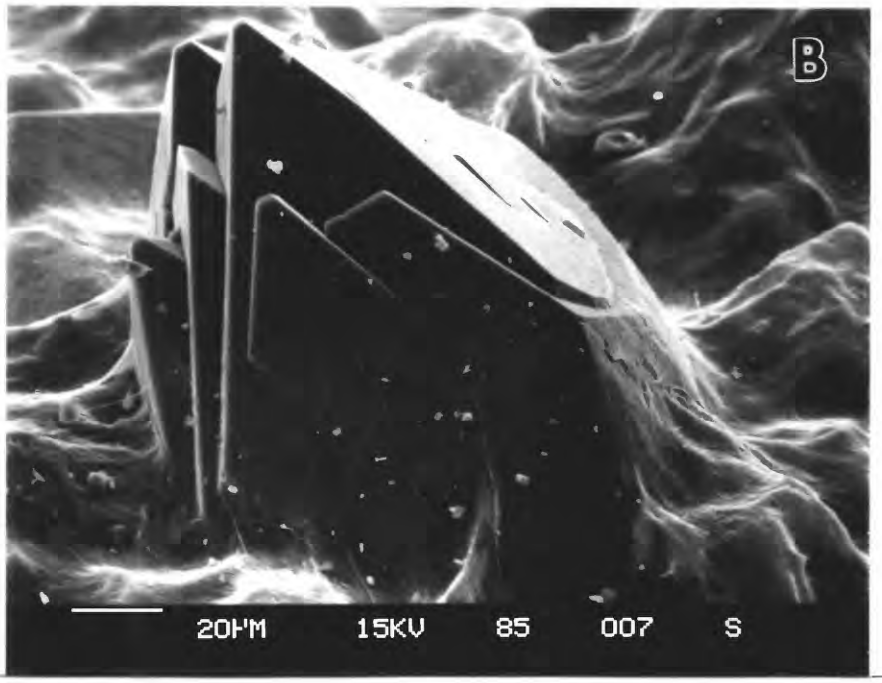

25. Scanning electron micrograph showing botryoidal clusters of platy crystals of an unidentified calcium silicate (EDS analysis) mineral that lines vesicles in core from 744.5-m depth in SOH-4.

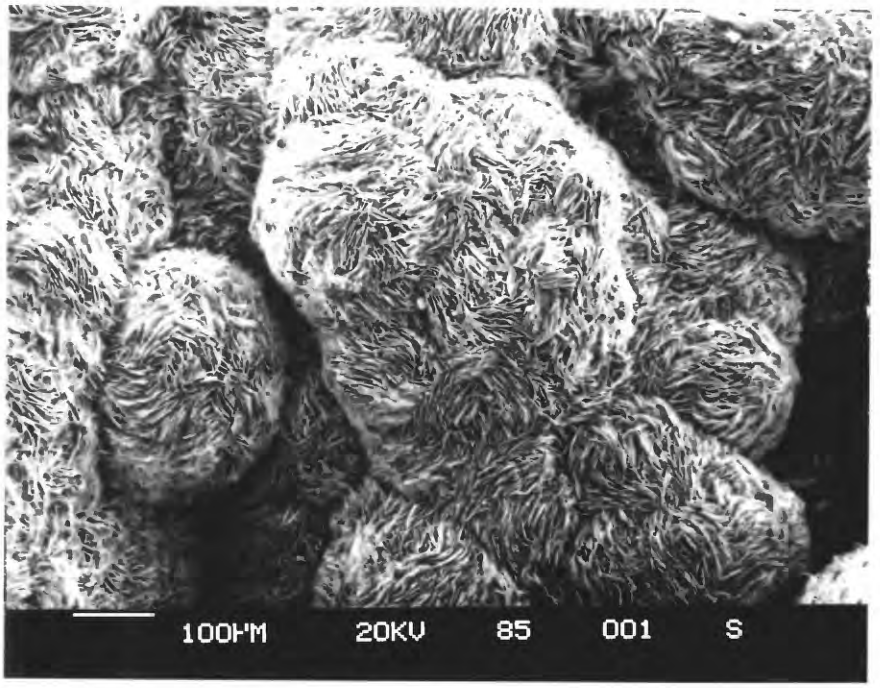

26. Scanning electron micrograph showing a honeycomb morphology typical of dark green, smectite, vesicle fillings (specimen is from 1,564.1-m depth in SOH-4).

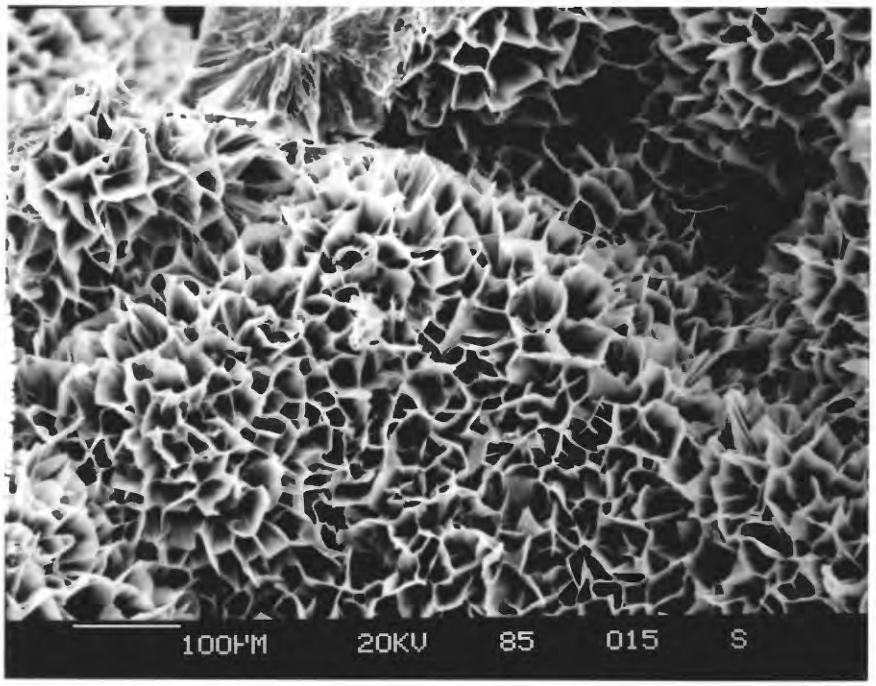

27. Scanning electron micrograph of bronze to red, tarnished, chalcopyrite cavity filling along with later, fibrous actinolite/tremolite(?); colorless, prismatic quartz; and green, platy, mixed-layer chlorite-smectite filling a cavity in core from 1,935.8-m depth in SOH-4.

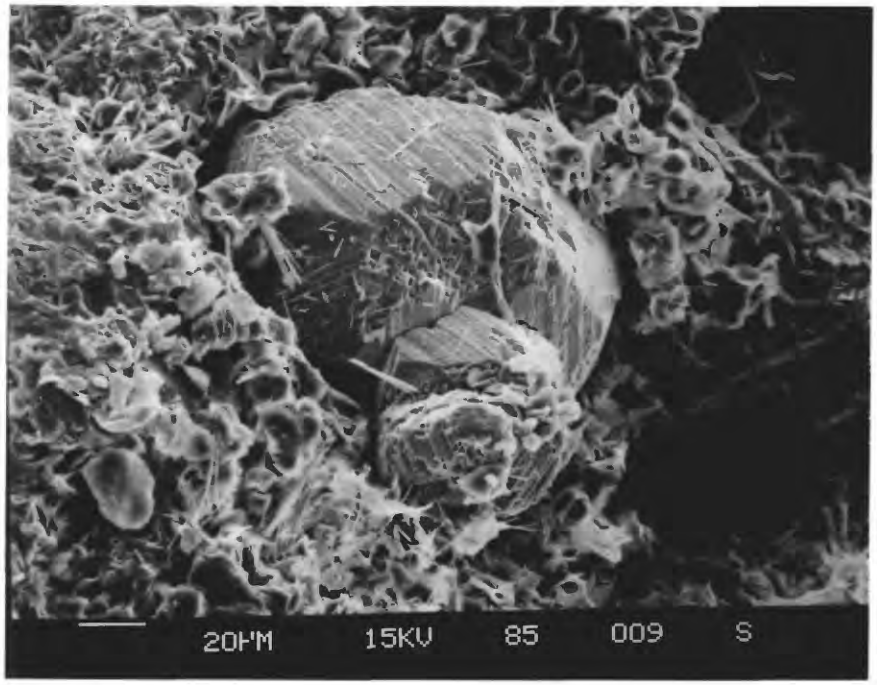

28. Scanning electron micrograph of white, rhombic adularia crystals lining vesicles, along with green smectite, in core from 1,302.8-m depth in SOH-4.

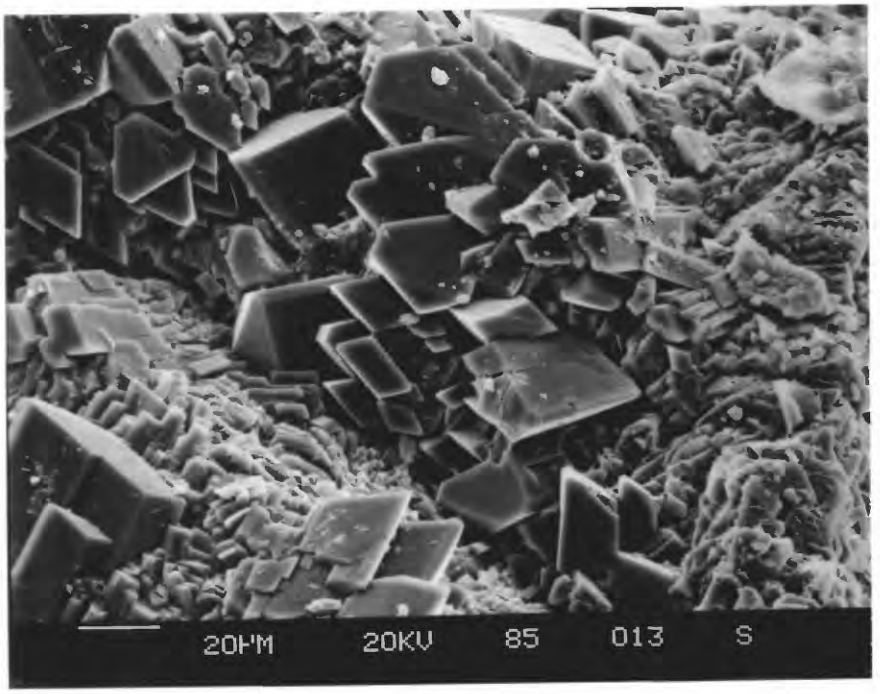

29. Scanning electron micrograph showing a cluster of colorless, plagioclase crystals filling a cavity at 1,734.6-m depth in SOH-4; the plagioclase crystals are sprinkled with particles of clay, broken plagioclase fragments, and particles resembling bacteria.

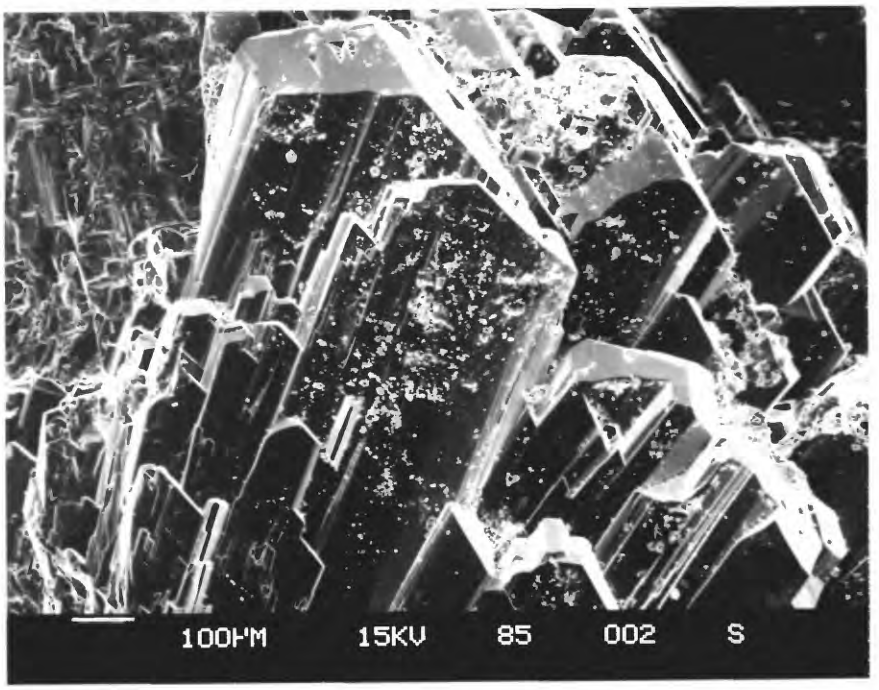

30. Scanning electron micrograph showing dimpled, bacteria-like particles that were located on plagioclase crystals (see Fig. 29) filling a cavity in core from 1,734.6-m depth in SOH-4. The nearly transparent connecting "trail" between the two particles at the left of the SEM probably consists of a viscous slime that permits adsorption and shows movement of the particle across the plagioclase crystal surface.

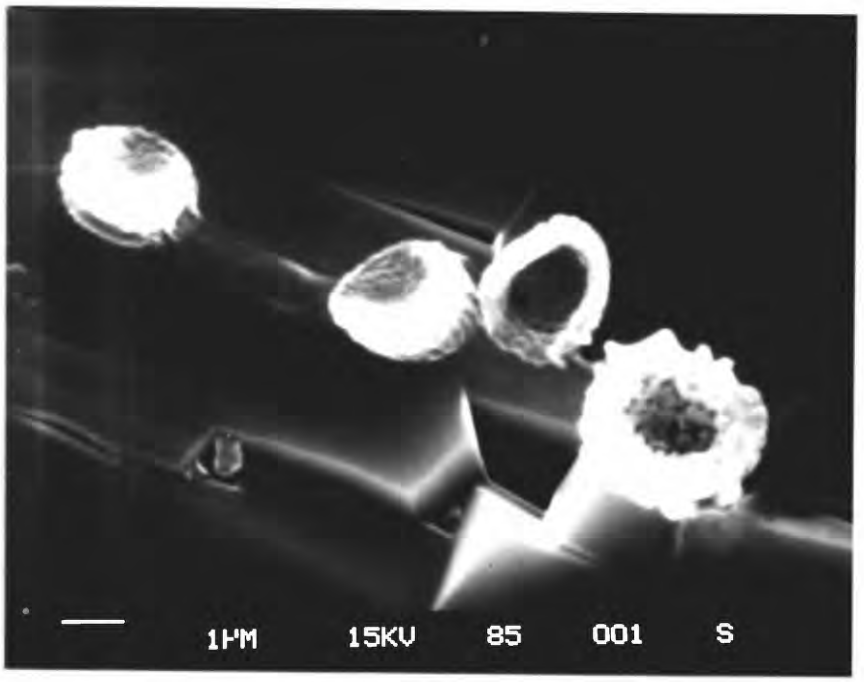

31. Scanning electron micrograph showing cubic pyrite deposited later than colorless, euhedral quartz crystals and before green, platy smectite on a fracture surface in core from 1,676.1-m depth in SOH-4.

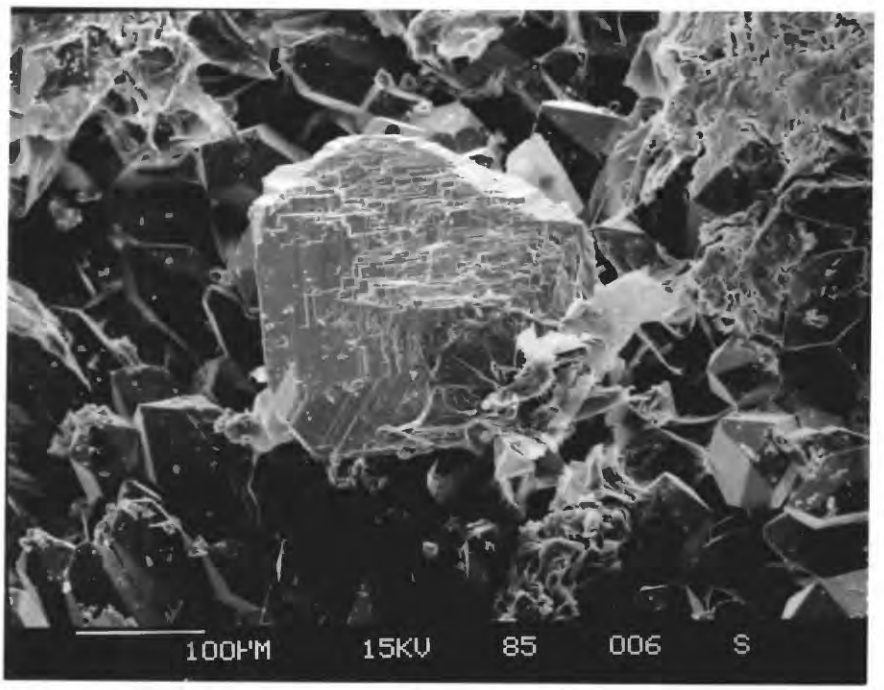

32. Scanning electron micrograph of bronze, tabular, hexagonal, pyrrhotite crystals coating a fracture along with earlier green smectite in core from 1,281.5-m depth in SOH-4.

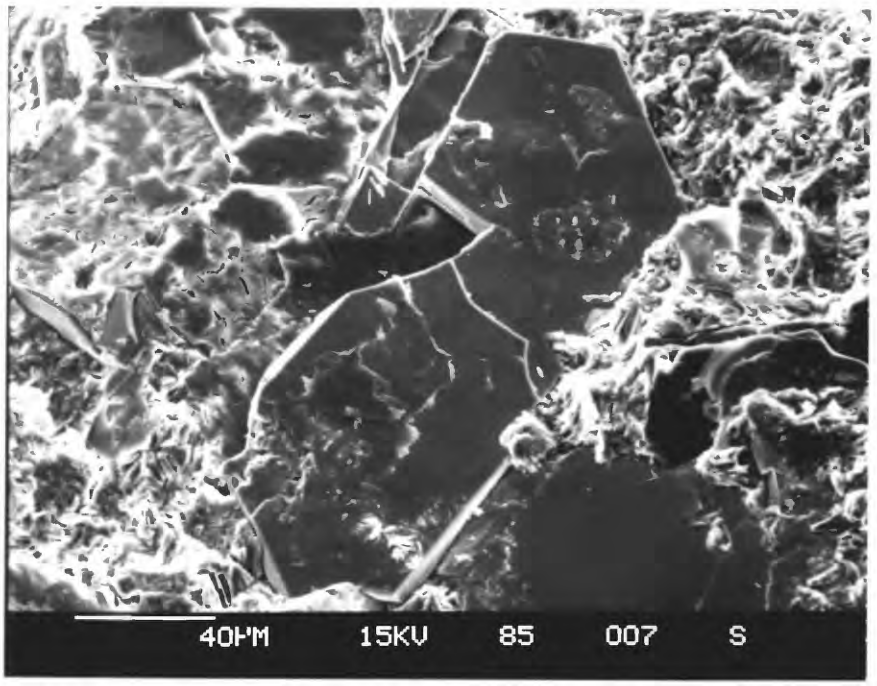

33. Scanning electron micrograph showing a cavity filling of colorless, euhedral, quartz crystals; dark-green, platy, mixed-layer chlorite-smectite; and white, fibrous, actinolite/tremolite(?) in core from 1,935.8-m depth in SOH-4.

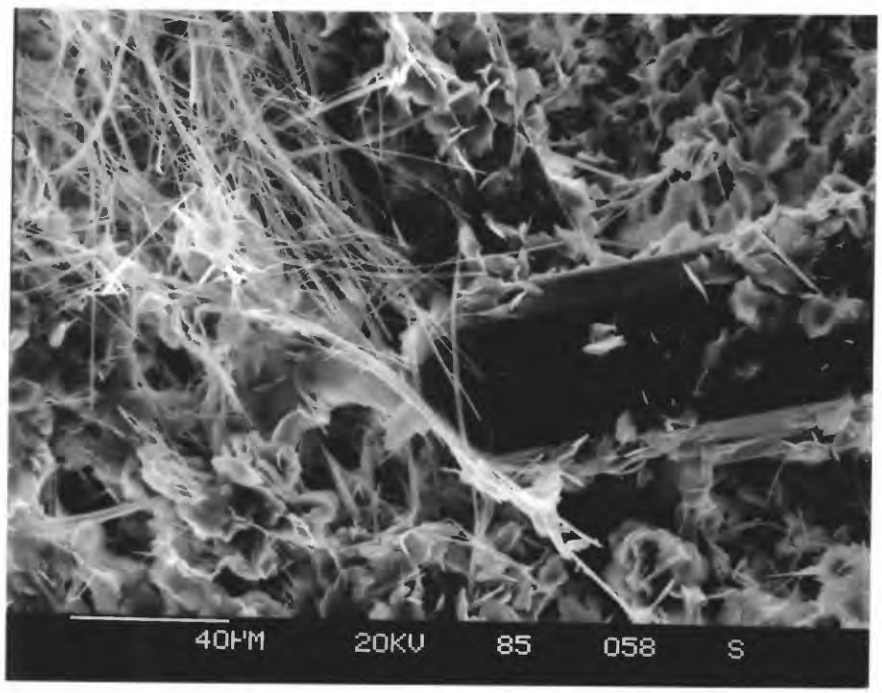

34. Scanning electron microgaraph of euhedral, light green epidote (Ep) crystals; later, colorless, quartz (Q) crystals; and still later dusting of dark green, chlorite-smectite filling spaces between breccia fragments in core from 1,971.3-m depth in SOH-4.

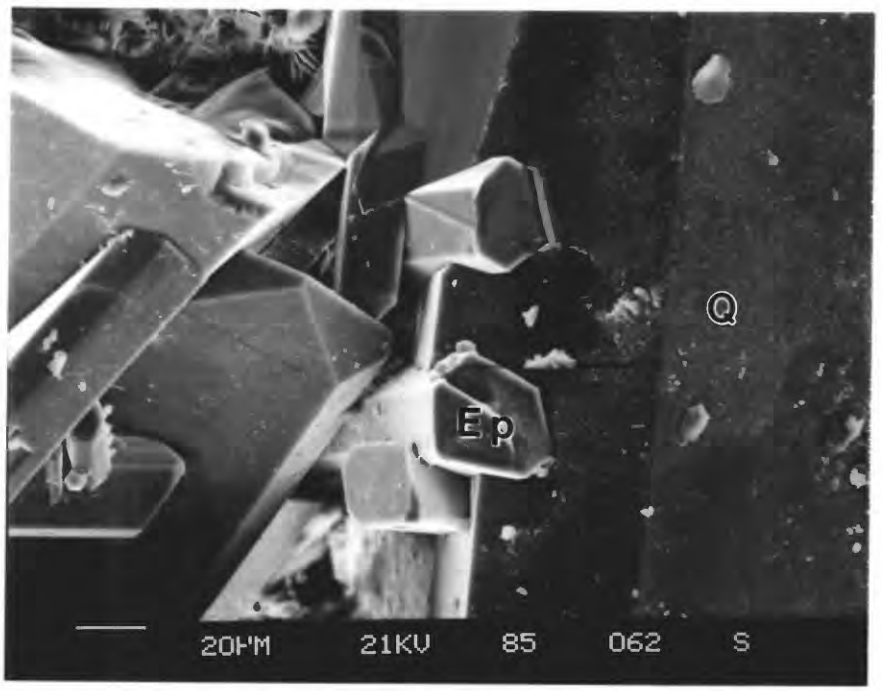

35. Plot of depth vs. T_h measurements for anhydrite and quartz fluid inclusion data from two depths in the SOH-1 drill hole (see Table 5). Solid curve is a measured-temperature with depth curve after Novak and Evans (1991). T_h measurements are shown by histograms (N = number of T_h measurements) with sample depth as the baseline.

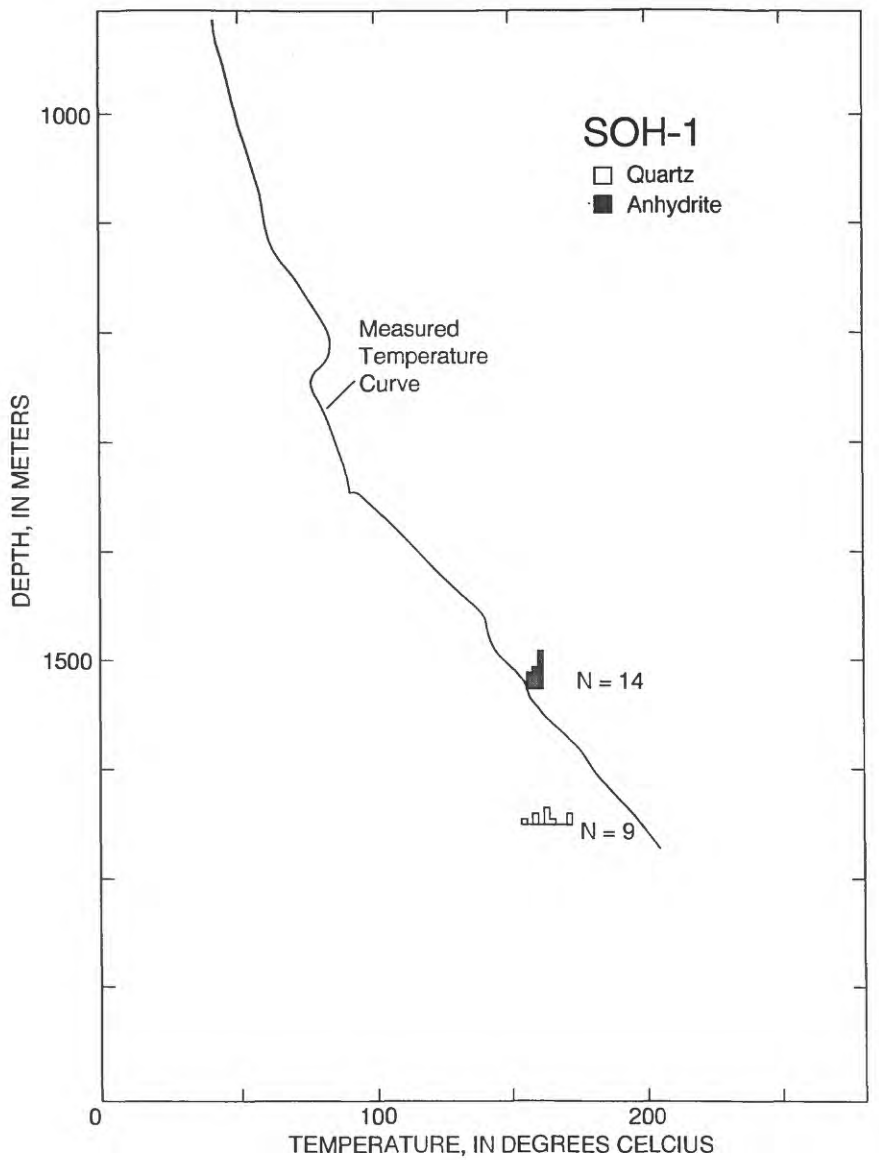

36. Plot of depth vs. T_h measurements for hydrothermal quartz fluid inclusion data from five depths in the SOH-2 drill hole (see Table 5). Dashed curve is a theoretical reference boiling point with depth curve after Elder (1981, Table A5). Solid curve shows the measured drill-hole temperatures (Evans, 1992). T_h measurements are plotted as histograms with sample depth as a baseline; N is the number of T_h measurements.

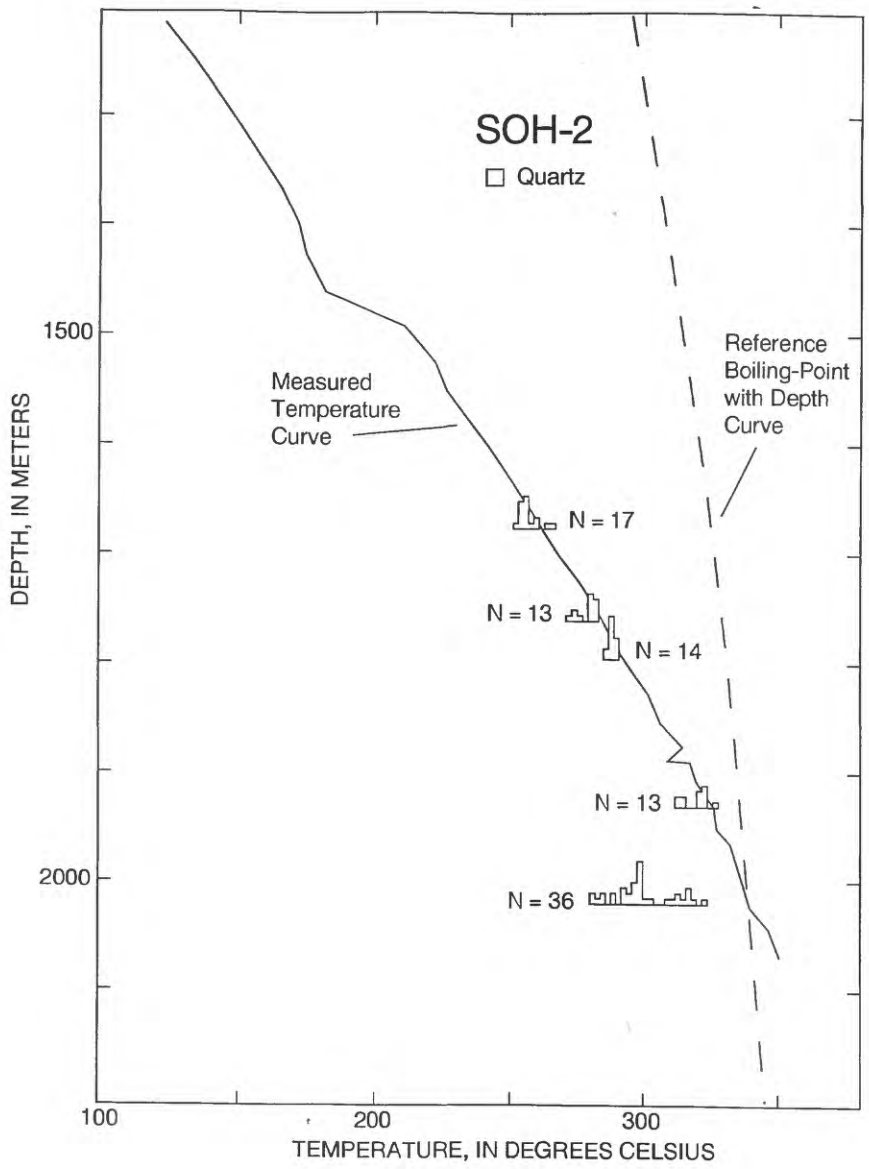

37. A. Photomicrographs of (A) liquid-rich, secondary(?), and (B) monophase vapor and vapor-rich fluid inclusions in hydrothermal quartz crystals from 2,019.8-m depth in SOH-2.

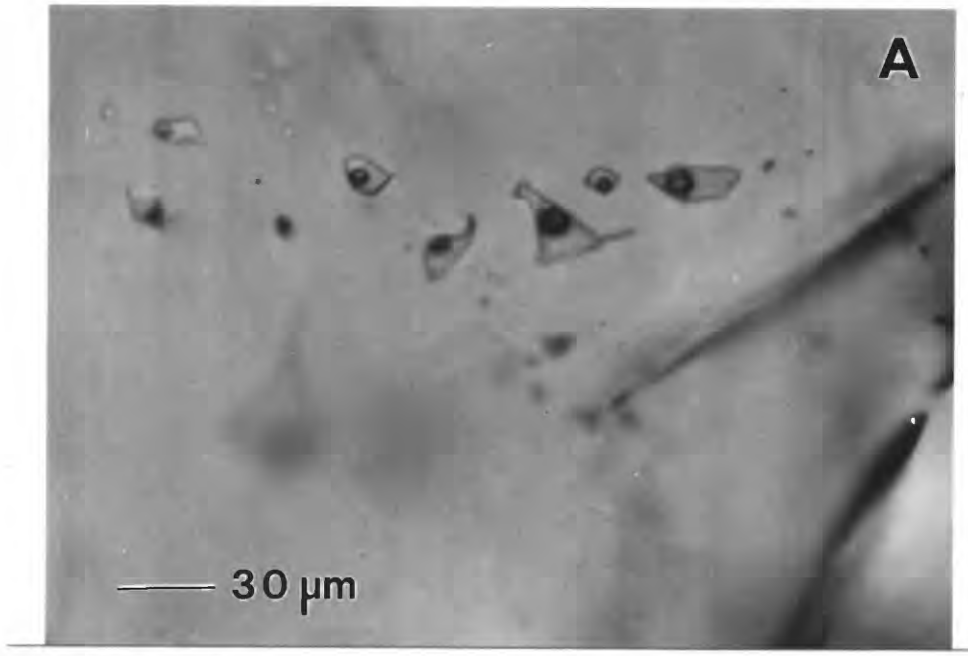

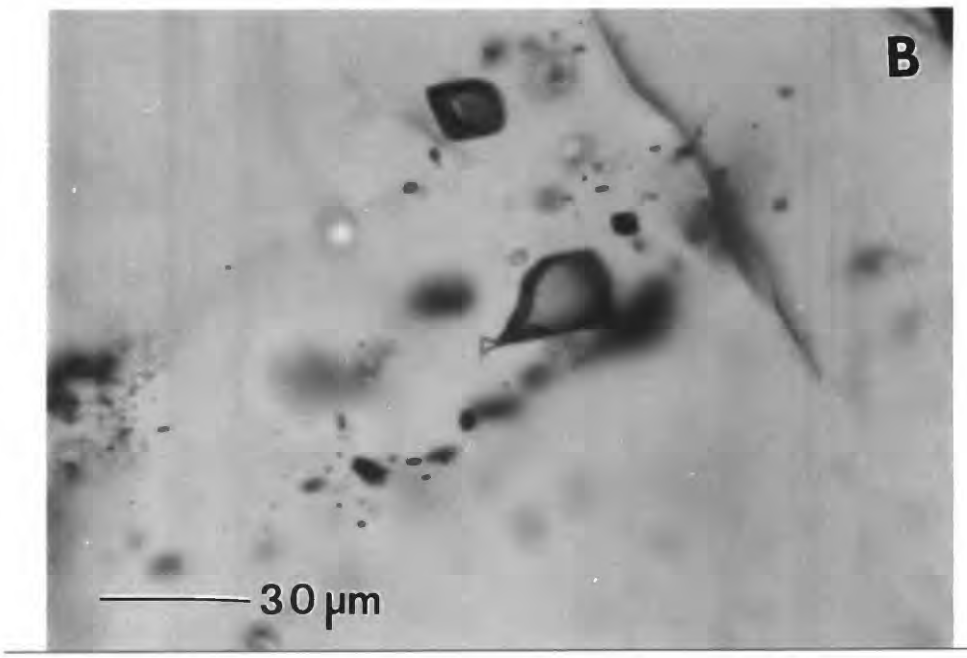

38. Plot of T_h measurements vs. salinity (calculated from T_m data) for fluid inclusions in hydrothermal anhydrite, calcite, and quartz crystals from the SOH drill holes.

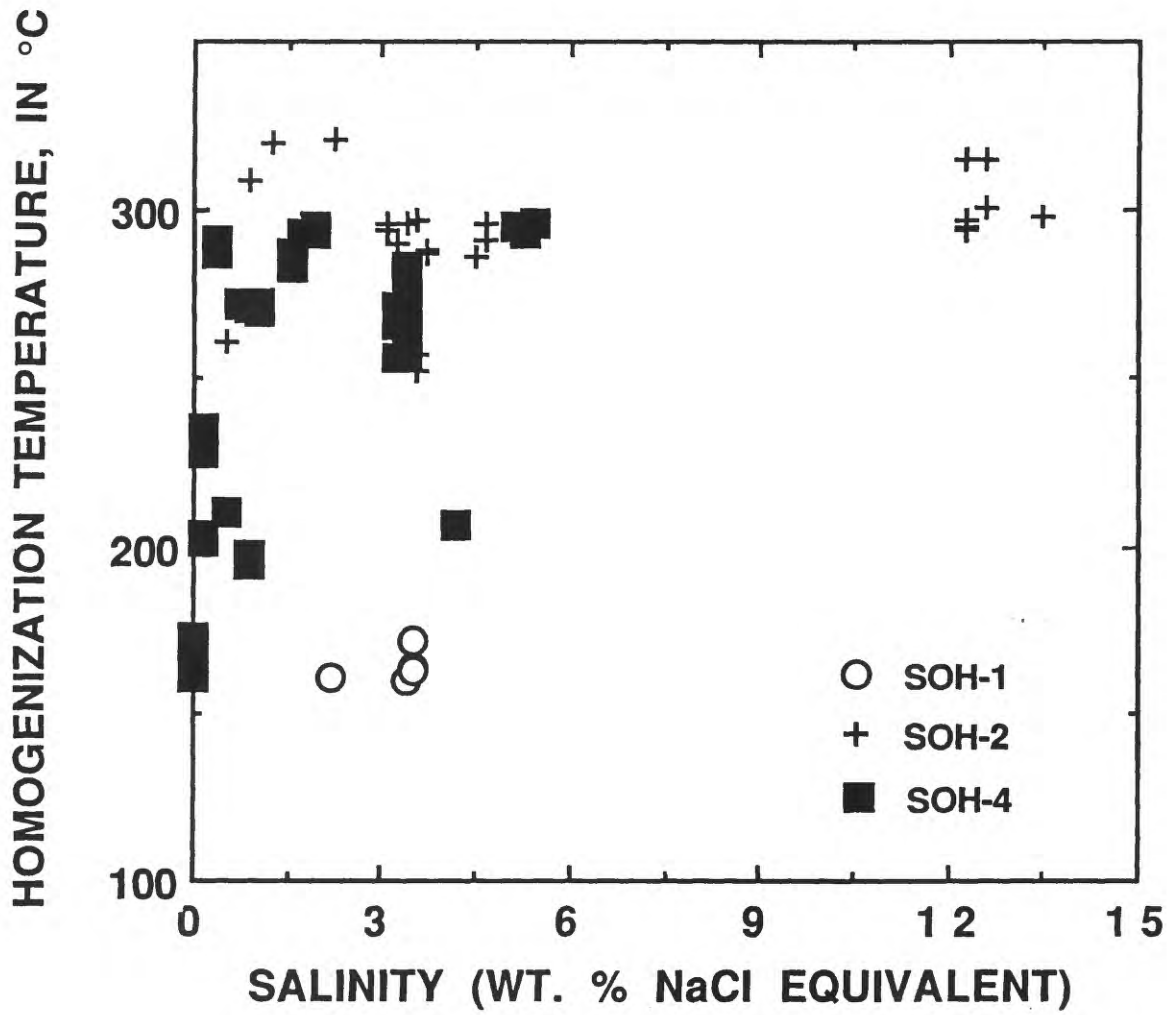

39. Plot of depth below mean sea level vs. salinity (from melting-point temperature data) of fluid inclusions from the SOH drill holes.

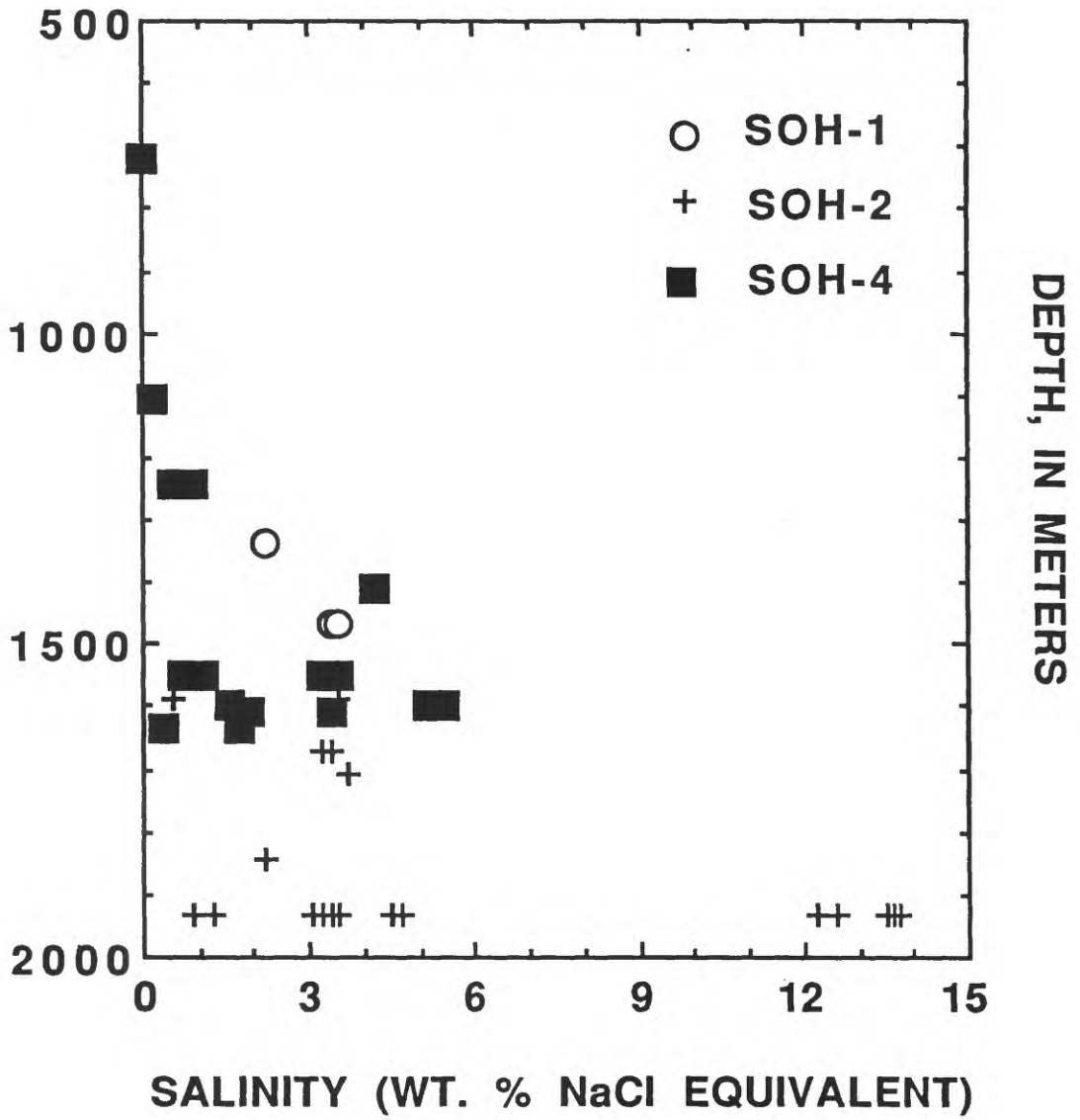

40. Plot of depth beneath the ground surface vs. T_h measurements of fluid inclusions in hydrothermal anhydrite, calcite, and quartz crystals from ten locations in SOH-4 (Table 5). Dashed curve is a theoretical reference boiling point with depth curve for pure water originating at the ground surface (after data in Table A5 of Elder, 1981). Dotted curve is a theoretical reference boiling-point curve for pure water originating at 1 km beneath the present ground surface. Solid curve shows the measured drill-hole temperatures for SOH-4 (after Novak and Evans, 1991). T_h measurements (N = number of measurements) are plotted as histograms with sample depth as a baseline.

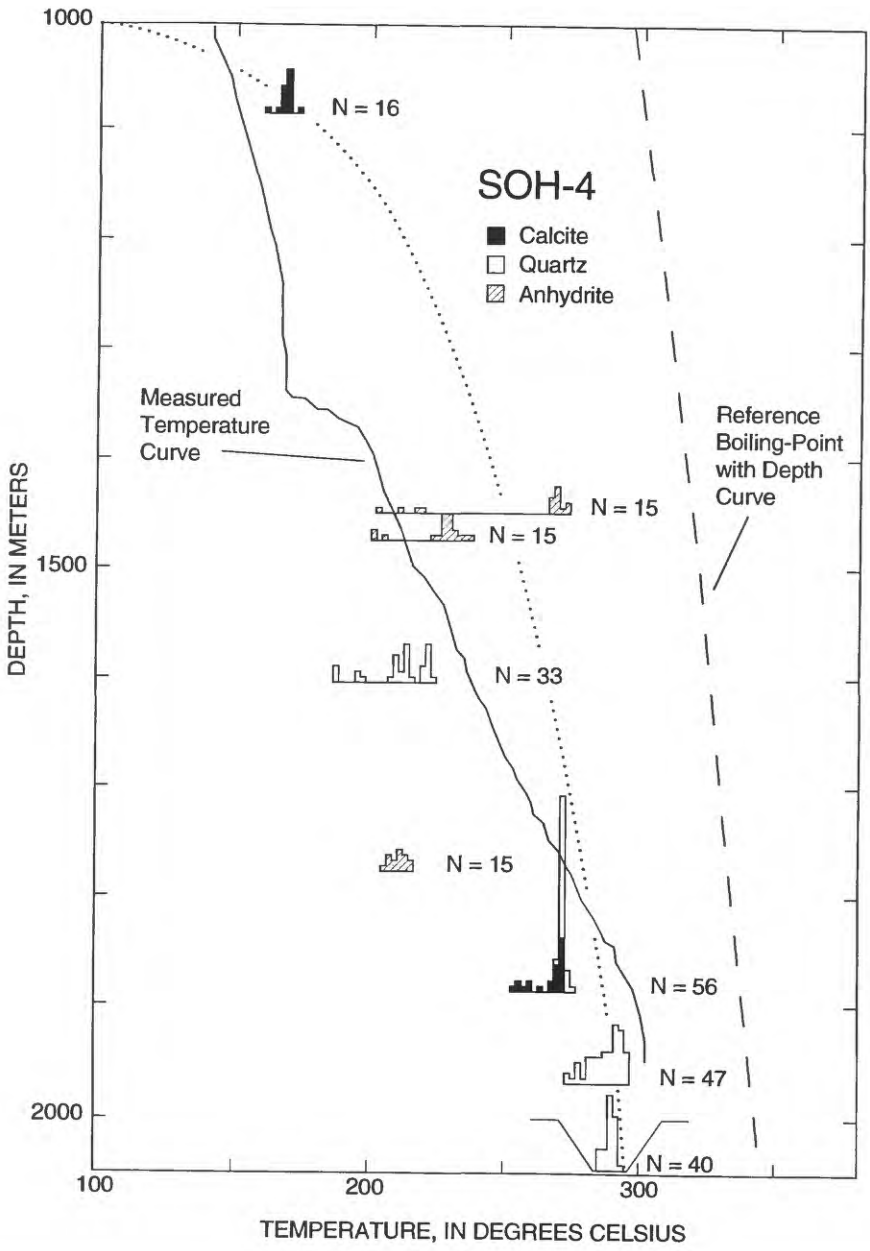

41. Photomicrographs of fluid inclusions from drill hole SOH-4 showing: A. liquid-rich, secondary fluid inclusions in calcite from 1,886.4-m depth; B. liquid-rich, secondary fluid inclusions in anhydrite from 1,771.7-m depth;

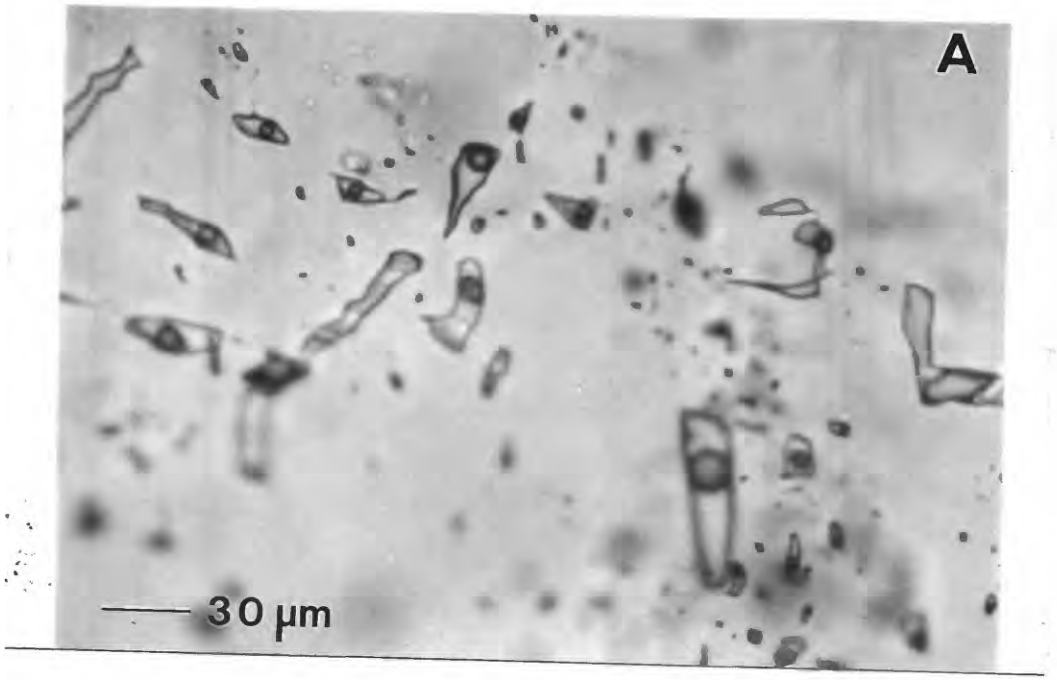

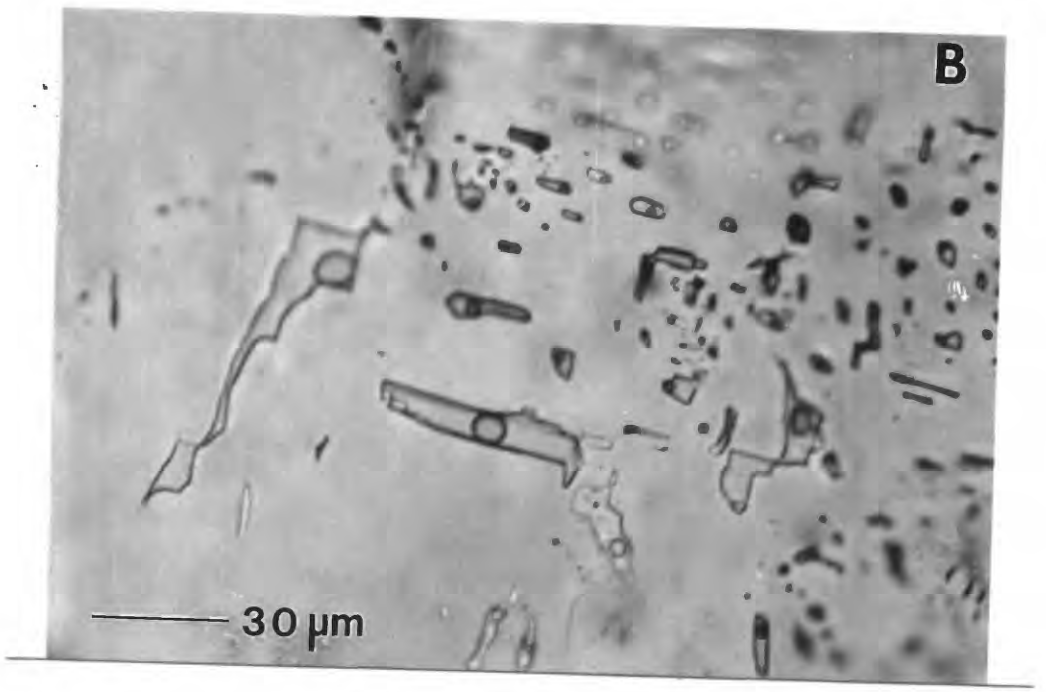

41. C. liquid-rich, secondary and vapor-rich (secondary or primary?) fluid inclusions in quartz from 1,959.7-m depth.

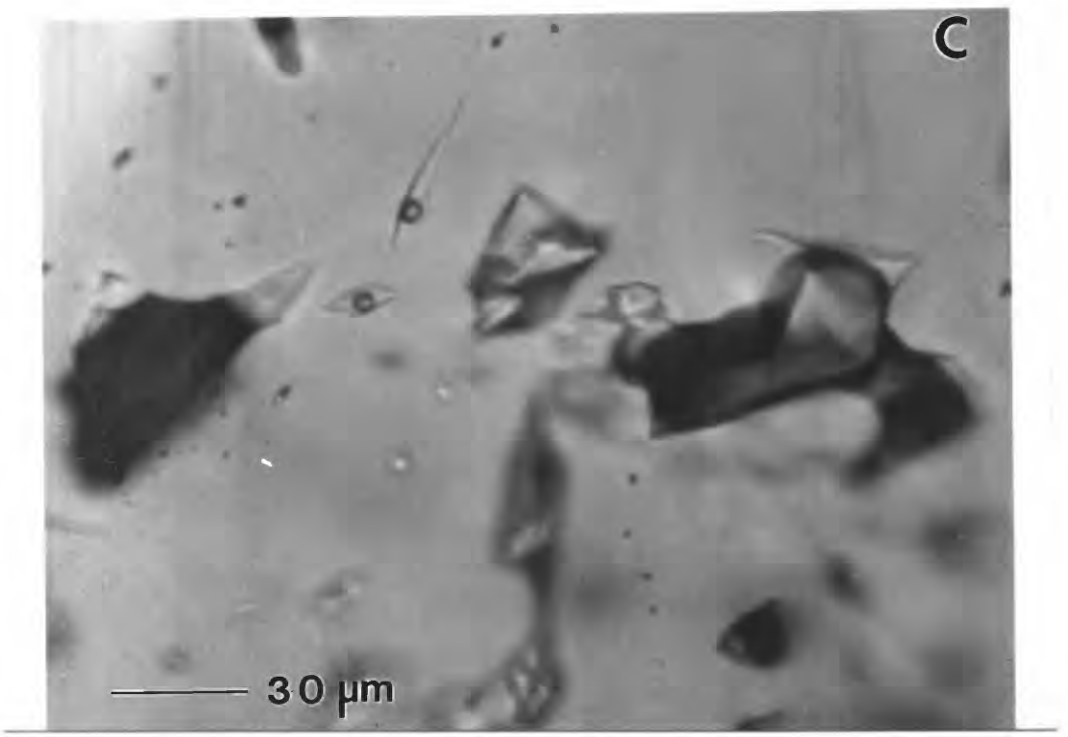

Table 1. Electron microprobe analyses of analcime from the SOH drill holes.

Sample no.	SOH-2 4108.8			SOH-4 5131				
Analysis no.	1	2	3	1	2	3	4	5
Major-element chemical analyses (weight percent oxides)								
SiO_2	54.63	53.98	54.46	56.04	54.41	55.95	56.28	56.05
Al_2O_3	23.72	24.06	23.94	22.96	23.06	22.71	22.65	22.67
Fe_2O_3	0.00	0.00	0.04	0.00	0.00	0.00	0.00	0.01
MgO	0.01	0.00	0.00	0.02	0.00	0.01	0.00	0.00
MnO	0.00	0.00	0.00	0.01	0.00	0.03	0.00	0.02
CaO	0.43	0.51	0.51	0.92	0.88	0.93	1.28	1.24
SrO	0.11	0.04	0.02	0.00	0.02	0.05	0.07	0.02
BaO	0.01	0.13	0.00	0.05	0.02	0.00	0.00	0.00
Na_2O	14.17	14.18	14.31	12.90	12.89	12.45	12.70	12.67
K_2O	0.04	0.03	0.02	0.07	0.06	0.05	0.05	0.06
Total	93.12	92.93	93.30	92.97	91.34	92.18	93.03	92.74
Number of atoms on the basis of 96 oxygens								
Si	31.69	31.43	31.55	32.36	32.03	32.51	32.48	32.44
Al	16.22	16.51	16.35	15.63	16.00	15.56	15.41	15.47
Fe	0.00	0.00	0.02	0.00	0.00	0.00	0.00	0.01
Mg	0.01	0.00	0.00	0.01	0.00	0.01	0.00	0.00
Mn	0.00	0.00	0.00	0.01	0.00	0.02	0.00	0.01
Ca	0.26	0.32	0.31	0.57	0.56	0.58	0.79	0.77
Sr	0.04	0.01	0.01	0.00	0.01	0.02	0.02	0.01
Ba	0.00	0.03	0.00	0.01	0.00	0.00	0.00	0.00
Na	15.93	16.01	16.08	14.44	14.72	14.03	14.21	14.22
K	0.03	0.02	0.01	0.05	0.04	0.04	0.04	0.04
Si+Al	47.91	47.94	47.90	47.98	48.03	48.06	47.89	47.91
$Si/Al+Fe^{3+}$	1.95	1.90	1.93	2.07	2.00	2.09	2.11	2.10
$Si/Si+Al+Fe^{3+}$	0.66	0.66	0.66	0.67	0.67	0.68	0.68	0.68
Balance Error[1]	-2.23	-1.50	-2.22	-1.18	0.68	1.63	-2.88	2.29

[1]Determined by method of Passaglia (1970)

Table 2. Electron microprobe analyses of feldspars from the SOH drill holes.

Sample no.	SOH-2 5846.7					SOH-4 5131			SOH-4 5691					
Mineral	Adularia								Albite					
Analysis no.	1	2	3	4	5	1	2	3	1	2	3	4	5	6
Major-element chemical analyses (weight percent oxides)														
SiO_2	65.92	66.82	65.74	65.15	65.83	65.21	65.16	65.69	67.39	67.44	66.46	68.24	67.46	68.50
Al_2O_3	18.21	18.22	18.27	17.86	18.30	18.95	18.89	19.01	22.04	22.18	21.41	21.45	21.97	20.98
Fe_2O_3	0.00	0.00	0.01	0.02	0.06	0.02	0.03	0.08	0.00	0.04	0.03	0.03	0.00	0.00
MgO	0.00	0.00	0.00	0.00	0.01	0.01	0.00	0.00	0.01	0.00	0.00	0.00	0.00	0.01
MnO	0.00	0.00	0.00	0.00	0.02	0.00	0.00	0.00	0.03	0.05	0.00	0.00	0.00	0.02
CaO	0.00	0.00	0.00	0.01	0.05	0.00	0.14	0.00	1.12	1.24	1.12	0.87	1.10	0.70
SrO	0.00	0.02	0.02	0.02	0.00	0.29	0.05	0.19	0.09	0.05	0.09	0.14	0.07	0.00
BaO	0.16	0.09	0.04	0.08	0.11	0.40	0.27	0.46	0.00	0.08	0.11	0.00	0.07	0.04
Na_2O	0.33	0.37	0.27	0.34	0.54	0.69	1.21	0.41	11.08	10.79	11.52	11.59	11.21	11.87
K_2O	15.30	15.81	15.82	15.23	15.68	15.81	14.82	15.76	0.07	0.03	0.06	0.07	0.09	0.04
Total	99.92	101.33	100.17	98.71	100.60	101.38	100.57	101.60	101.83	101.90	100.80	102.39	101.97	102.16
Number of atoms on the basis of 32 oxygens														
Si	12.11	12.13	12.08	12.12	12.06	11.92	11.94	11.96	11.61	11.60	11.60	11.69	11.61	11.76
Al	3.94	3.90	3.96	3.92	3.95	4.08	4.08	4.08	4.47	4.50	4.41	4.33	4.46	4.25
Fe	0.00	0.00	0.00	0.00	0.01	0.00	0.00	0.01	0.00	0.01	0.00	0.00	0.00	0.00
Mg	0.00	0.00	0.00	0.00	0.00	0.00	0.00	0.00	0.00	0.00	0.00	0.00	0.00	0.00
Mn	0.00	0.00	0.00	0.00	0.00	0.00	0.00	0.00	0.00	0.01	0.00	0.00	0.00	0.00
Ca	0.00	0.00	0.00	0.00	0.01	0.00	0.03	0.00	0.21	0.23	0.21	0.16	0.20	0.13
Sr	0.00	0.00	0.00	0.00	0.00	0.03	0.01	0.02	0.00	0.01	0.01	0.01	0.01	0.00
Ba	0.01	0.01	0.00	0.01	0.01	0.03	0.02	0.03	0.01	0.01	0.01	0.00	0.00	0.00
Na	0.12	0.13	0.10	0.12	0.19	0.25	0.43	0.14	3.70	3.60	3.90	3.85	3.74	3.95
K	3.59	3.66	3.71	3.62	3.66	3.69	3.46	3.66	0.01	0.01	0.01	0.02	0.02	0.01

Table 3. Electron microprobe analyses of smectite and mixed-layer chlorite-smectite from the SOH drill holes.

Sample no.	SOH-2 4108.8		SOH-2 4508.5				SOH-2 5846.7			SOH-4 5691.0		
Mineral	Smectite						Chlorite-smectite			Smectite		
Analysis no.	1	2	1	2	3	4	1	2	3	1	2	3
Major-element chemical analyses (weight percent oxides)												
SiO_2	42.29	41.70	43.43	44.45	43.18	44.67	47.31	50.57	38.22	45.29	43.22	41.55
Al_2O_3	9.44	8.23	8.31	8.42	8.37	8.20	11.20	11.05	8.39	7.73	7.08	6.94
Fe_2O_3	12.94	12.29	18.88	19.91	19.12	20.49	9.60	9.01	15.56	12.49	11.49	11.38
MgO	16.56	17.38	14.54	14.31	14.28	15.17	5.43	4.09	9.93	19.90	18.18	17.82
MnO	0.14	0.13	0.08	0.11	0.14	0.07	0.17	0.21	0.15	0.12	0.09	0.05
CaO	2.01	1.53	2.80	2.66	2.23	2.76	3.94	5.50	5.32	0.92	1.00	0.93
SrO	0.04	0.00	0.06	0.10	0.04	0.03	0.01	0.00	0.01	0.08	0.03	0.07
BaO	0.07	0.00	0.00	0.05	0.03	0.09	0.03	0.13	0.00	0.00	0.00	0.02
Na_2O	0.99	1.24	0.61	0.72	0.61	0.96	0.66	1.05	0.52	0.88	0.56	0.75
K_2O	0.07	0.05	0.10	0.12	0.12	0.09	2.72	2.56	0.44	0.07	0.07	0.04
Total	84.55	82.55	88.81	90.85	88.12	92.53	81.07	84.17	78.54	87.48	81.72	79.55
Number of atoms on the basis of 22 oxygens												
Si	6.47	6.52	6.44	6.46	6.45	6.40	7.43	7.64	6.46	6.64	6.76	6.69
Al	1.53	1.48	1.45	1.44	1.47	1.39	0.57	0.36	1.54	1.34	1.24	1.31
Al	0.17	0.04	—	—	—	—	2.13	1.61	0.13	—	0.06	.01
Fe	1.49	1.45	2.11	2.18	2.15	2.21	1.13	1.02	1.98	1.38	1.35	1.38
Mg	3.77	4.05	3.22	3.10	3.18	3.24	1.27	0.92	2.50	4.35	4.23	4.28
Mn	0.02	0.02	0.10	0.01	0.02	0.01	0.02	0.03	0.02	0.01	0.01	0.01
Ca	0.33	0.26	0.45	0.41	0.36	0.42	0.66	0.89	0.96	0.15	0.17	0.32
Sr	0.00	0.00	0.01	0.01	0.00	0.00	0.00	0.00	0.00	0.01	0.00	0.01
Ba	0.00	0.00	0.00	0.00	0.00	0.01	0.00	0.01	0.00	0.00	0.00	0.00
Na	0.29	0.38	0.18	0.20	0.18	0.27	0.20	0.31	0.17	0.25	0.17	0.24
K	0.01	0.01	0.02	0.02	0.02	0.02	0.54	0.49	0.10	0.01	0.01	0.01

Table 4. Electron microprobe analyses of garnet and talc from the SOH-2 drill hole.

Sample no.	SOH-2 6714.1									
Mineral	Garnet					Talc				
Analysis no.	1	2	3	4	5	1	2	3	4	5
Major-element chemical analyses (weight percent oxides)										
SiO_2	36.92	36.69	36.34	36.41	36.76	59.14	59.75	59.73	59.50	59.58
Al_2O_3	2.27	3.83	3.31	3.25	2.59	1.59	1.43	1.39	1.32	1.33
Fe_2O_3	28.39	25.36	26.26	25.74	27.73	—	—	—	—	—
FeO	—	—	—	—	—	4.78	4.19	4.02	4.04	4.12
MgO	0.79	0.94	0.67	0.69	1.06	27.42	28.34	28.17	27.92	27.77
MnO	0.19	0.28	0.23	0.29	0.20	0.11	0.11	0.02	0.02	0.00
CaO	32.90	33.33	33.28	33.14	32.60	0.04	0.04	0.03	0.07	0.09
SrO	0.00	0.01	0.08	0.01	0.00	0.00	0.13	0.00	0.00	0.06
BaO	0.00	0.03	0.00	0.00	0.03	0.00	0.00	0.00	0.01	0.00
Na_2O	0.00	0.09	0.00	0.00	0.02	0.49	0.41	0.36	0.39	0.51
K_2O	0.04	0.03	0.02	0.03	0.04	0.08	0.06	0.05	0.06	0.06
Total	101.50	100.59	100.19	99.56	101.03	93.65	94.46	93.77	93.33	93.52
Number of atoms on the basis of 24 oxygens										
Si	6.18	6.02	6.01	6.05	6.04	8.13	8.18	8.22	8.23	8.22
Al	0.45	0.74	0.64	0.64	0.50	0.26	0.23	0.23	0.22	0.22
Fe^{3+}	3.22	3.13	3.27	3.22	3.43	—	—	—	—	—
Fe^{2+}	—	—	—	—	—	1.10	0.96	0.93	0.94	0.95
Mg	0.20	0.23	0.17	0.17	0.26	5.62	5.78	5.78	5.75	5.71
Mn	0.03	0.04	0.03	0.04	0.03	0.01	0.01	0.00	0.00	0.00
Ca	5.90	5.86	5.90	5.90	5.74	0.01	0.01	0.01	0.01	0.01
Sr	0.00	0.00	0.01	0.00	0.00	0.00	0.01	0.00	0.00	0.01
Ba	0.00	0.00	0.00	0.00	0.00	0.00	0.00	0.00	0.00	0.00
Na	0.00	0.03	0.00	0.00	0.01	0.13	0.11	0.10	0.10	0.14
K	0.01	0.01	0.00	0.04	0.01	0.01	0.01	0.01	0.01	0.01

Table 5. Fluid-inclusion heating and freezing data for hydrothermal minerals from the Kilauea ERZ SOH drill holes

Drill hole	Sample depth below ground surface (m)	Host mineral	Number of melting-point temperature measurements	Melting-point temperatures (°C)	Salinity (weight percent NaCl equivalent)	Number of homogenization temperature measurements	Range of homogenization temperatures (°C)	Mean homogenization temperature (°C)	Measured drill hole temperature (°C)
SOH-1									
	1526.8	Anhydrite	1	-1.3	2.2	14	157 - 161	160	157
	1654.9	Quartz	4	-2.0, -2.1	3.4, 3.6	9	155 - 171	163	200
SOH-2									
	1672.7	Quartz	3	-0.3, -2.1	0.5, 3.6	17	252 - 267	258	262
	1759.1	"	2	-1.9, -2.0	3.2, 3.4	13	270 - 282	278	284
	1791.7	"	2	-2.2	3.7	14	285 - 289	287	290
	1928.8	"	1	-1.3	2.2	13	312 - 326	318	324
	2019.8	"	20	-0.5 to -9.8	0.9 to 13.7	36	279 - 321	297	338
SOH-4									
	1085.4	Calcite	14	0.0	0.0	16	160 - 173	168	151
	1452.4	Anhydrite	0	—	—	15	204 - 272	254	208
	1472.5	"	5	-0.1	0.2	20	201 - 236	225	212
	1605.4	Quartz	3	-0.3, -0.5	0.5, 0.9	33	187 - 223	211	238
	1771.7	Anhydrite	1	-2.5	4.2	15	205 - 215	210	273
	1886.4	Calcite	15	-1.9 to -2.1	3.2 to 3.6	24	253 - 272	266	297
	"	Quartz	9	-0.4 to -0.6	0.7 to 1.1	32	269 - 275	271	297
	1959.7	"	14	-0.9, -3.1 to -3.3	1.6, 5.1 to 5.4	17	282 - 296	288	303
	1969.9	"	7	-2.0	3.4	30	273 - 291	284	304
	1973.9	"	4	-1.1	1.9	15	290 - 295	293	304
	1996.3	"	12	-0.2, -1.0	0.4, 1.7	40	284 - 293	288	306

Table 6. Approximate measured temperatures (in °C) at which hydrothermal minerals occur in the Kilauea ERZ SOH drill holes compared with drill holes in Iceland and other geothermal areas

Mineral	SOH-1	SOH-2	SOH-4	Iceland[1]	Other areas[2]
Analcime	<50-205	134-300	<100-265	<100-300	
Chabazite	<50-60			<75	
Erionite		138			<110
Heulandite	133-165		<100-152	60-170	
Mordenite	120-206	160-270	70-152	80-230	
Phillipsite	<50-60		70	60-85	
Wairakite			265	180-300	
Apophyllite			70		?
Gyrolite	<50-133			<200	
Truscottite	110-185	240	226-265	<200	
Tobermorite		138-165	230	24-149	
Xonotlite			230-260		?
Aragonite	<40-42				?
Calcite	<40-206	170-347	<100-305	<270	<100-350
Smectite	40-206	<60-340	<100-306	<200	<150
Chlorite-smectite		173-349	158-298	200-240	100-200
Chlorite		270-349	260-306	<100-240+	<100-350
Kaolinite-serpentine		214			?
Talc	175	295-350	290-302		290-320
Opal			<100	<90	
Cristobalite	165-200		126-150		<100-210
Chalcedony	156-205	167-349	150-290	<100	<40-240
Quartz	156-206	175-349	154-306	100-300+	150-300+
Adularia		134-302	148-252		150-300+
Albite		176-265	228-304	220-300	100-350
Prehnite			230-232	210-240	220-350
Epidote		285-338	304	>230-300+	220-350
Actinolite-Tremolite		324-349	300-302	280+	260-400
Biotite(?)		326			270-340+
Garnet		322			250-300+
Anhydrite	93-185	138-348	222-306	60-300	
Gypsum	<40-93	168-177	<100-222		<70
Pyrite	<40-205	<60-349	100-255	<100-350+	100-300+
Chalcopyrite		302-326	298-306		250-350
Pyrrhotite		334	167		150-350
Galena		302			280-320
Sphalerite		302			
Hematite		290-338	<100-246		<100-250

[1] from:
Tómasson and Kristmannsdóttir (1972)
Kristmannsdóttir (1975)
Kristmannsdóttir and Tómasson (1978)
Kristmannsdóttir (1979)
Jakobsson and Moore (1986)
Fridleifsson (1991)

[2] from:
Honda and Muffler (1970)
Keith *et al.* (1978)
Holland and Malinin (1979)
Elders *et al.* (1979)
Cavarretta *et al.* (1982)
Leach et al. (1983)
Aumento and Liguori (1986)
Hulen and Nielson (1986)
White *et al.* (1988)